




CDK9 and PP2A regulate RNA polymerase II transcription termination and coupled RNA maturation

Michael Tellier^{1,*} , Justyna Zaborowska¹, Jonathan Neve², Takayuki Nojima³, Svenja Hester², Marjorie Fournier², Andre Furger²  & Shona Murphy^{1,**} 

Abstract

CDK9 is a kinase critical for the productive transcription of protein-coding genes by RNA polymerase II (pol II). As part of P-TEFb, CDK9 phosphorylates the carboxyl-terminal domain (CTD) of pol II and elongation factors, which allows pol II to elongate past the early elongation checkpoint (EEC) encountered soon after initiation. We show that, in addition to halting pol II at the EEC, loss of CDK9 activity causes premature termination of transcription across the last exon, loss of polyadenylation factors from chromatin, and loss of polyadenylation of nascent transcripts. Inhibition of the phosphatase PP2A abrogates the premature termination and loss of polyadenylation caused by CDK9 inhibition, indicating that this kinase/phosphatase pair regulates transcription elongation and RNA processing at the end of protein-coding genes. We also confirm the splicing factor SF3B1 as a target of CDK9 and show that SF3B1 in complex with polyadenylation factors is lost from chromatin after CDK9 inhibition. These results emphasize the important roles that CDK9 plays in coupling transcription elongation and termination to RNA maturation downstream of the EEC.

Keywords CDK9; mRNA cleavage and polyadenylation complex; PP2A; RNA polymerase II; transcription

Subject Categories Chromatin, Transcription, & Genomics

DOI 10.15252/embr.202154520 | Received 15 December 2021 | Revised 13 July 2022 | Accepted 21 July 2022 | Published online 18 August 2022

EMBO Reports (2022) 23: e54520

Introduction

Transcription of human protein-coding genes by RNA polymerase (pol) II is a complex process comprising initiation, elongation, and termination. In addition, mRNA capping, splicing, and cleavage and polyadenylation, which are required to produce a mature mRNA, are largely cotranscriptional (Tellier *et al.*, 2020a). The dynamic

phosphorylation and dephosphorylation of proteins that control transcription and pre-mRNA processing, including pol II itself, are fundamental to the regulation of gene expression. Phosphorylation of pol II mostly occurs on the carboxyl-terminal domain (CTD) of its largest subunit, RBP1, which comprises 52 repeats of the heptapeptide sequence Tyr1,Ser2,Pro3,Thr4,Ser5,Pro6,Ser7 (YSPTSPS) (Zaborowska *et al.*, 2016). During transcription, tyrosine, serine, and threonine residues are reversibly and dynamically phosphorylated while the two prolines are subject to cis-trans isomerization. The pattern of heptapeptide phosphorylation and proline isomerization during the transcription process creates distinct CTD profiles throughout the transcription cycle to coordinate the recruitment of transcription elongation and pre-mRNA processing factors in space and time (Buratowski, 2009; Hsin & Manley, 2012; Corden, 2013; Zaborowska *et al.*, 2016). For example, CTD Ser5 phosphorylation helps to recruit capping proteins at the 5' end of genes and Ser2 phosphorylation helps to recruit polyadenylation and termination factors at the 3' end of genes.

In human cells, phosphorylation of the pol II CTD heptapeptide is mainly carried out by cyclin-dependent kinases (CDKs), including CDK7, CDK9, and CDK12 (Zaborowska *et al.*, 2016). CDK9, together with Cyclin T1, forms the positive transcription elongation factor b complex (P-TEFb), which phosphorylates Ser2, Thr4, and Ser5 of the CTD heptapeptide. In addition, P-TEFb phosphorylates several proteins involved in regulation of transcriptional elongation, including the negative elongation factor subunit E (NELFE), the SPT5 subunit of DSIF, and SPT6 (Peterlin & Price, 2006; Yamada *et al.*, 2006; Vos *et al.*, 2018a, 2018b). Soon after initiation of transcription of protein-coding genes, pol II stalls at an early elongation checkpoint (EEC) due to the recruitment of NELF and DSIF. Phosphorylation of these complexes by P-TEFb results in release of NELF and turns DSIF into a positive elongation factor, allowing productive elongation to proceed (Jonkers *et al.*, 2014; Laitem *et al.*, 2015; Vos *et al.*, 2018a, 2018b). Accordingly, inhibition of CDK9 by small molecule inhibitors causes pol II to pause at the EEC genome-wide (Jonkers *et al.*, 2014; Laitem *et al.*, 2015; Vos *et al.*, 2018a, 2018b). Using

1 Sir William Dunn School of Pathology, University of Oxford, Oxford, UK

2 Department of Biochemistry, University of Oxford, Oxford, UK

3 Medical Institute of Bioregulation, Kyushu University, Fukuoka, Japan

*Corresponding author. Tel: +44 1865275583; E-mail: michael.tellier@path.ox.ac.uk

**Corresponding author. Tel: +44 1865275551; E-mail: shona.murphy@path.ox.ac.uk

short-term treatment of cells with CDK9 inhibitors, we have shown that inhibition of CDK9 also disrupts transcription at the 3' end of protein-coding genes, causing premature termination of pol II close to the poly(A) site (Laitem *et al*, 2015). This premature termination is accompanied by the loss of several pol II-associated factors, including CDK9 itself, SPT5, SSU72, and Cstf64 from the 3' end of protein-coding genes (Laitem *et al*, 2015). This led us to hypothesize the presence of a poly(A)-associated checkpoint (PAAC), where CDK9 is required to overcome the pause and transcribe past the poly(A) site for cleavage and polyadenylation to occur (Laitem *et al*, 2015; Tellier *et al*, 2016).

Termination of transcription downstream of an active polyadenylation site requires the action of the exonuclease Xrn2, which degrades the uncapped RNA left associated with pol II after cleavage of the nascent pre-mRNA at the poly(A) site (Kim *et al*, 2004; West *et al*, 2004; Proudfoot, 2016). This is thought to destabilize pol II to allow termination of transcription. Interestingly, phosphorylation of Xrn2 by CDK9 enhances its activity (Sanso *et al*, 2016).

As the functions of transcriptional kinases are becoming clearer, thanks in part to the development of cell lines with analog-sensitive kinases (Bishop *et al*, 2000; Tellier *et al*, 2020b), the role of phosphatases in this process are beginning to emerge. Several CDK9 targets, including SPT5 and Xrn2, are dephosphorylated by the multifunctional protein phosphatases (PP)1, PP2A, and PP4 (Parua *et al*, 2018, 2020; Huang *et al*, 2020; Vervoort *et al*, 2021), which also have roles in splicing (Mermoud *et al*, 1992; Shi *et al*, 2006). In addition, PP1 was recently shown to regulate poly(A)-site-dependent transcription termination by dephosphorylation of SPT5 (Cortazar *et al*, 2019; Eaton *et al*, 2020). Knockdown of PP1 or its associated subunit, PNUTS, or inhibition of PP1 with the small molecule inhibitor Tautomycin, leads to hyperphosphorylation of SPT5 and the elongation rate of pol II no longer decreases downstream of the poly(A). This leads to a transcription termination defect as the exonuclease Xrn2 fails to “catch up” with the elongating pol II (Cortazar *et al*, 2019; Eaton *et al*, 2020). PP2A interacts with Integrator, a protein complex that cleaves RNA and regulates the amount of paused pol II at the EEC (Huang *et al*, 2020; Zheng *et al*, 2020; Vervoort *et al*, 2021). PP2A is also thought to dephosphorylate the pol II CTD and other factors involved in the early stages of transcription (Huang *et al*, 2020; Zheng *et al*, 2020; Vervoort *et al*, 2021).

There is also evidence that termination of transcription of intron-containing protein-coding genes in human cells is coupled to terminal exon definition, which requires the coordinated recognition of the 3'SS and the poly(A) site (Cooke *et al*, 1999; Tellier *et al*, 2020a). For example, mutation of the 3'SS causes a transcription termination defect due to failure to recognize the poly(A) site (Dye & Proudfoot, 1999). Interactions between splicing factors, such as SF3B1 or U2AF65, and CPA factors, such as CPSF100 or poly(A) polymerase, PAPOLA, have been demonstrated (Niwa *et al*, 1990; Gunderson *et al*, 1994; Vagner *et al*, 2000; Kyburz *et al*, 2006; Tellier *et al*, 2020a). In addition, subunit CDC73 of the PAF complex, which plays a role in elongation, interacts with the CPSF73 CPA endonuclease (Rozenblatt-Rosen *et al*, 2009). Thus, inhibition of CDK9 may trigger premature termination by disrupting the balance of kinase and phosphatase activities required for enabling protein-protein/-DNA/-RNA interactions.

To elucidate the function of CDK9 in the PAAC, we generated, using CRISPR/Cas9, a HEK293 cell line where the endogenous genes

express analog-sensitive CDK9 (CDK9as). Inhibition of CDK9as or small molecule CDK9 inhibitors promote premature termination of pol II, impair CPA factor recruitment to chromatin, and cause loss of polyadenylation of newly made pre-mRNA. Interestingly, bioinformatic analysis indicates that the defect in transcription caused by CDK9 inhibition starts across the last exon, rather than at the poly(A) site, implicating disruption of definition of the last exon in premature termination.

Using phosphoproteomics, we have identified numerous targets of CDK9 including, as expected, SPT5 and NELF, in addition to the U2 snRNP splicing factor component SF3B1, with SF3B1 T142P confirmed as a PP1 target. Inhibition of CDK9 does not affect interaction between CPA factors and the SF3B complex but rather promotes the loss of interaction between pol II and a complex containing SF3B and CPA factors, suggesting that CDK9 plays a role in the recruitment of these factors to the elongation complex at the end of genes. PP1 inhibition promotes a transcription termination defect, as previously shown (Eaton *et al*, 2020) but does not reverse the effect of CDK9 inhibition on transcription and pol II CTD phosphorylation. However, inhibition of PP2A reverses the effect of CDK9 inhibition on premature termination, indicating that this phosphatase has a previously unsuspected role at the 3' end of protein-coding genes. Inhibition of PP2A also restores recruitment of poly(A) factors and the polyadenylation of newly made pre-mRNA disrupted by CDK9 inhibition. PP2A inhibition alone causes an increase in pol II signal across the last exon, a greater recruitment of SF3B1 to the pol II complex, and a higher production of polyadenylated mRNA indicating that PP2A is a negative regulator of mRNA CPA.

Taken together, our results highlight an additional kinase/phosphatase switch at the end of protein-coding genes regulating the coordination of pre-mRNA splicing, cleavage/polyadenylation, and termination of transcription.

Results

CDK9 inhibition abrogates polyadenylation

We have previously shown that CDK9 inhibition leads to loss of pol II-association downstream of the poly(A) site of human protein-coding genes (Laitem *et al*, 2015). This premature termination of transcription could be accompanied by loss of polyadenylation and failure to make a mature mRNA. Alternatively, polyadenylation/termination may be more efficient and fully mature mRNA produced. We have already shown that levels of the polyadenylation factor CstF64 at the 3' end of genes are reduced after CDK9 inhibition, suggesting that polyadenylation is compromised. To follow the production of newly polyadenylated mRNA, we have analyzed production of transcripts from TNF α -inducible genes. HeLa cells were treated with DMSO or TNF α for 30 min followed by treatment with DMSO or 5,6-dichlorobenzimidazole-1- β -D-ribofuranoside (DRB) for 30 min and 3'READS was then carried out on the purified nuclear mRNAs to measure the production of newly polyadenylated mRNA (Fig 1A; Neve *et al*, 2016). There are 307 genes where mRNA production is induced more than twofold by TNF α in both repeats. Pol II ChIP-qPCR on one of these genes, *LDLR*, was carried out to analyze induction of transcription by TNF α and the effect of

DRB treatment on pol II at the 3' end (Appendix Fig S1A). Polyadenylation of the 307 TNF α -induced mRNAs in the nucleus is significantly decreased, both for all of the genes included and for genes longer than 40 kb, where pol II is still elongating at the 3' end (Fig 1B and Appendix Fig S1A). qRT-PCR of the nuclear polyadenylated mRNAs encoded by selected TNF α -induced genes confirmed

that DRB causes a marked reduction in polyadenylation (Appendix Fig S1B).

We also performed Western blotting to assess the level of the polyadenylation/termination factors Xrn2, CPSF2, CPSF73, total pol II, and CTD Ser2P in chromatin and nucleoplasm after treatment of HeLa cells for 15 or 30 min with DRB (Fig 1C–E and

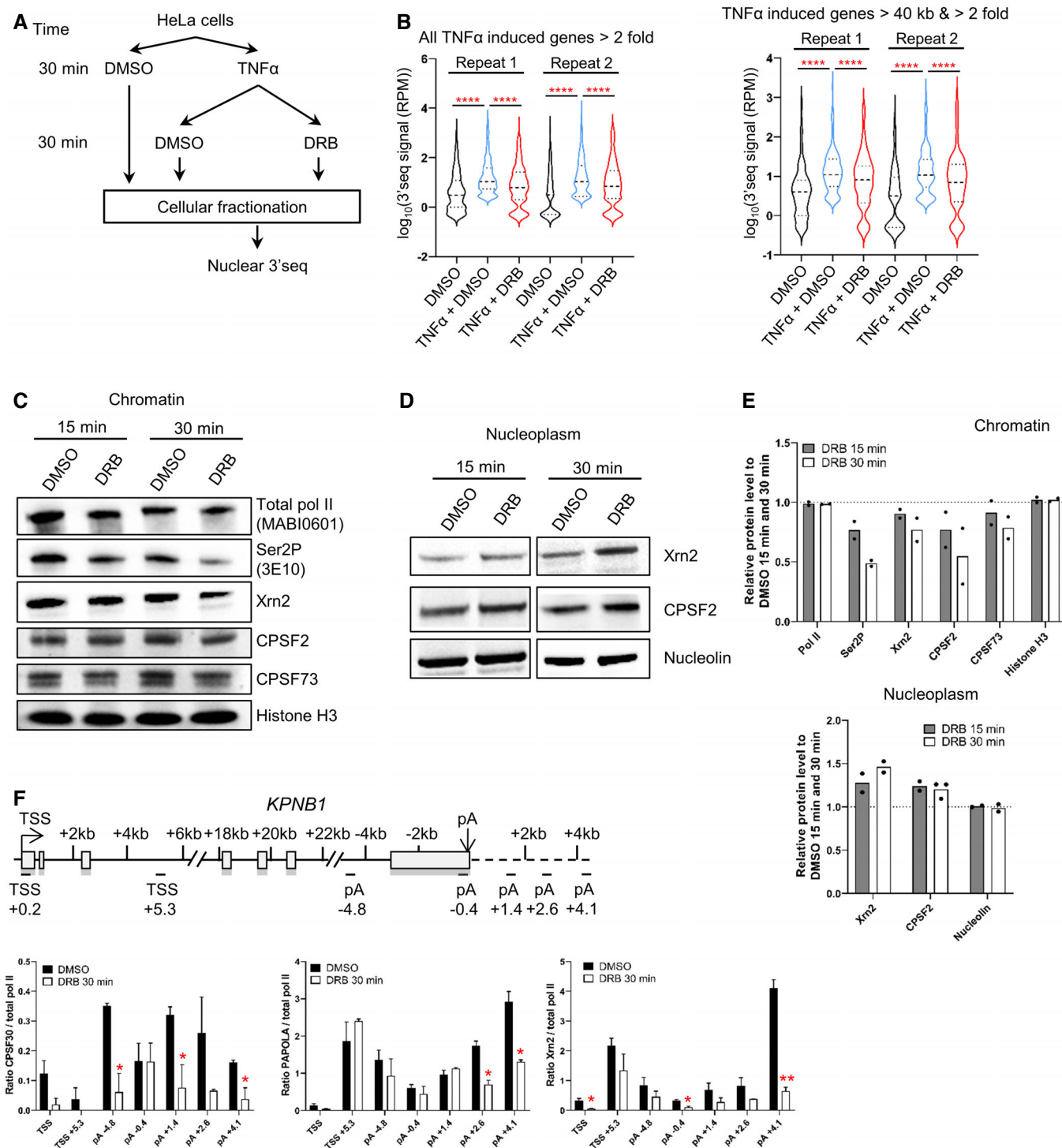


Figure 1.

Figure 1. CDK9 inhibition abrogates polyadenylation.

- A Schematic of the nuclear 3'READS experiment.
- B Violin plots of the 3'READS signal on all the TNF α induced genes ($n = 307$) or the set of TNF α induced genes longer than 40 kb ($n = 111$). **** $P < 0.0001$. Statistical test: Friedman test with Dunn's multiple test correction. Violin plot: minimal-to-maximal value, dashed horizontal line: median, dotted horizontal lines: interquartile (25 and 75%).
- C Western blot of total pol II, Ser2P, Xrn2, CPSF2, CPSF73, and histone H3 as a loading control, on the chromatin fraction.
- D Western blot of Xrn2, CPSF2, and Nucleolin as a loading control, on the nucleoplasm fraction (the CPSF73 antibody does not provide reliable results on the nucleoplasm fraction).
- E Quantification of the western blots shown in C and D. $n = 2$ biological replicates, mean.
- F Ratio of the different CPA and termination factors to total pol II. $n = 3$ biological replicates, mean \pm SEM, P -value: * $P < 0.05$, ** $P < 0.01$. Statistical test: two-tailed unpaired t -test.

Appendix Fig S1C). As expected, Ser2P is decreased on the chromatin following CDK9 inhibition. There is also loss of Xrn2, CPSF2 and CPSF73 from the chromatin fraction, with a greater loss after 30 than 15 min. In contrast, the level of these factors in the nucleoplasm fraction increases, indicating that these factors dissociate from chromatin after CDK9 inhibition. Importantly, there is no reduction in these factors in whole-cell extract, indicating that the loss from chromatin is not due to active degradation (Appendix Fig S1D and E). Levels of the poly(A) polymerase (PAPOLA), Xrn2 and CPSF30, measured by ChIP-qPCR on our model gene, *KPNB1*, which is approximately 35 kb long with two major poly(A) sites, are also reduced after 30-min treatment with DRB, whether ratioed to pol II levels or not (Fig 1F and Appendix Fig S1F and G).

This data indicate that CDK9 inhibition causes both premature termination of pol II and failure to recruit polyadenylation factors, which causes the production of polyadenylated mRNA to be aborted.

CDK9 inhibition causes an elongation defect starting at the last exon of protein-coding genes

To better understand the kinetics of premature termination of pol II caused by CDK9 inhibition, mNET-seq was carried out with a total pol II antibody after treatment of HeLa cells with DRB for 5, 10, 15, or 30 min (Figs 2A–C and EV1A and B). The results are similar to those we previously obtained using GRO-seq (Laitem *et al.*, 2015). Metagene profile analysis indicates that DRB treatment of cells causes an increase in pol II pausing close to the TSS and a loss of pol II entering productive elongation. In addition, premature termination of pol II close to the poly(A) site is detected on genes longer than 40 kb where pol II has not yet “run off” (Figs 2B–D and EV1A and B). Pol II ChIP-qPCR on *KPNB1* after treatment of cells with DRB concentrations between 12.5 and 100 μ M gives the same result (Fig EV1C). Interestingly, these data also show that CDK9 inhibition

affects pol II at the EEC more rapidly (easily detectable after 5-min inhibition) than at the 3' end of genes (only detectable after 10-min inhibition).

To focus on the effect of CDK9 inhibition on pol II behavior at the 3' end of genes, a metagene analysis was carried out with the pol II signal scaled across the last exon (Fig 2E). Interestingly, the metaprofile indicates that CDK9 inhibition causes an increase in pol II signal across the last exon followed by loss of pol II signal downstream of the poly(A) site. Importantly, the increase in the pol II signal after CDK9 inhibition is specific to the last exon as the pol II signal over the penultimate exons or other internal exons is either unchanged or decreased (Figs 2F and EV1D). This is particularly apparent on, for example, *ARHGAP23* where pol II levels increase specifically across the last exon (Fig 2G).

These findings indicate that the defect in transcription at the 3' end of genes caused by CDK9 inhibition starts upstream of the poly (A) site and occurs more slowly than loss of transcription at the EEC.

Inhibition of analog-sensitive (as) CDK9 has the same effect on elongation as small molecule CDK9 inhibitors

Small molecule kinase inhibitors may target more than one kinase *in vivo* (Bensaude, 2011). To confirm that the results we observed with DRB are due solely to inhibition of CDK9, we used CRISPR/Cas9 to change the gatekeeper phenylalanine to an alanine in all endogenous copies of CDK9 HEK293 cells to make a CDK9 analog-sensitive (as) cell line (Fig EV2A), which has a similar growth rate to the wild-type cells (Fig EV2B). Treatment of wild-type HEK293 or CDK9as cells with 7.5, 10, or 15 μ M of the ATP-analog 1-NA-PP1 (NA), which should specifically inhibit CDK9as (Zhang *et al.*, 2013), affects the growth rate of the CDK9as cells with little effect on the wild-type HEK293 cells (Fig EV2C). Pol II ChIP-qPCR of *KPNB1* in CDK9as cells after treatment of cells with 7.5, 10, or 15 μ M NA for

Figure 2. CDK9 inhibition causes an elongation defect starting at the last exon of protein-coding genes.

- A Schematic of the total pol II mNET-seq experiments.
- B Metagene profile of total pol II after 30-min treatment with DMSO (black) or DRB (green) around the TSS of expressed protein-coding genes ($n = 6,965$).
- C Metagene profile of total pol II after 30-min treatment with DMSO (black) or DRB (green) around the used poly(A) site of expressed protein-coding genes longer than 40 kb ($n = 2,816$).
- D Screenshot of the genome browser mNET-seq tracks across the protein-coding gene *KPNB1*. Red arrows indicate increased pol II pausing, loss of pol II entering productive elongation, and premature termination.
- E Metagene profile of total pol II after 30-min treatment with DMSO (black) or DRB (green) around the used last exon of expressed protein-coding genes ($n = 2,526$).
- F Metagene profile of total pol II after 30-min treatment with DMSO (black) or DRB (green) around the penultimate exon of expressed protein-coding genes ($n = 2,426$).
- G Screenshot of the genome browser mNET-seq tracks at the 3' end of protein-coding gene *ARHGAP23*. The red arrow indicates increased pol II signal across the last exon.

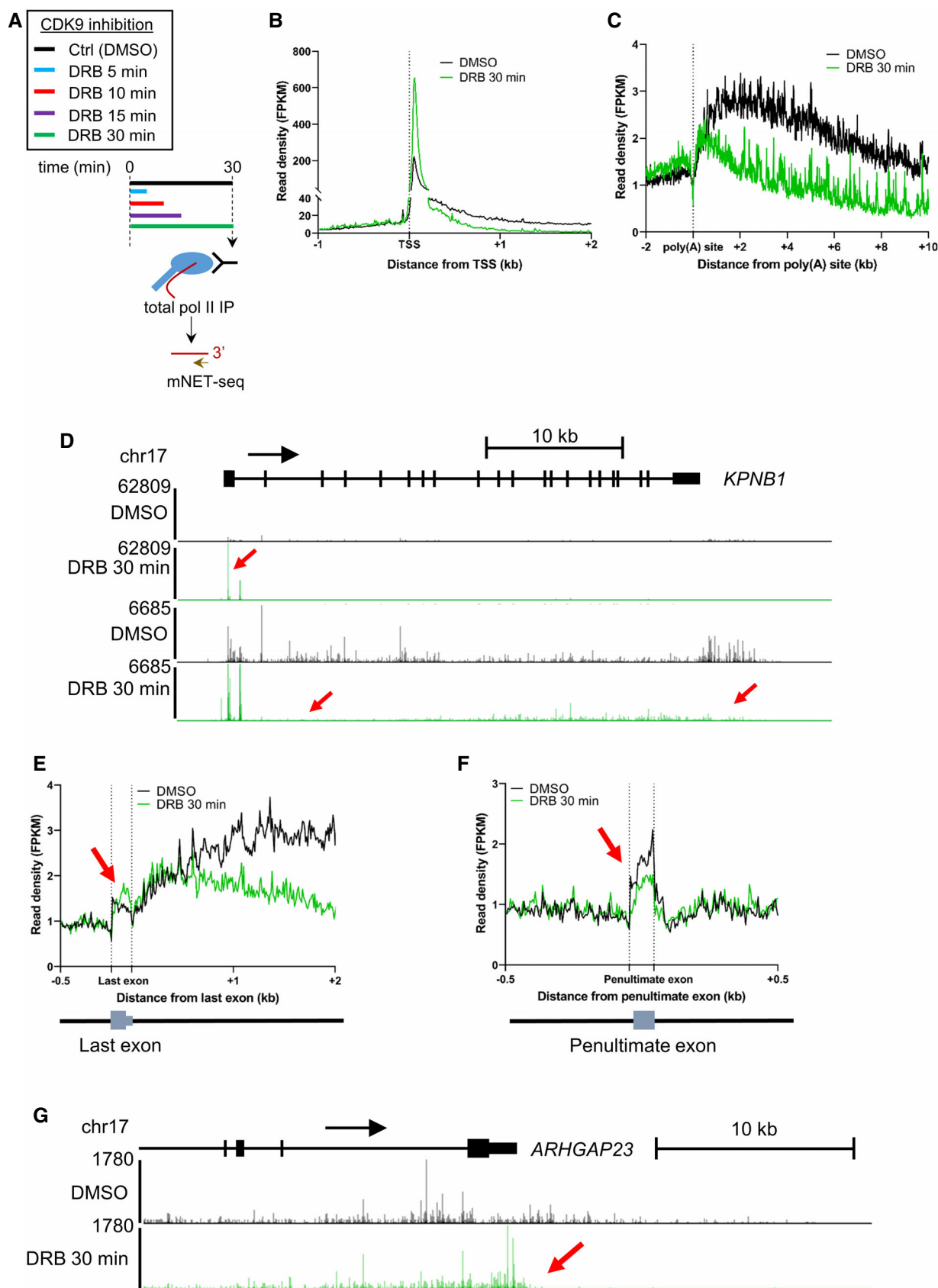


Figure 2.

15 min indicates that at all NA concentrations pol II pausing and pol II entry into productive elongation is affected (Fig EV2D). Readily detectable premature termination of pol II close to the poly(A) site is caused by 15 μ M NA (Fig EV2D). Importantly, 15 μ M NA has no effect on pol II in wild-type HEK293 (Fig EV2E). Introduction of the CDK9as mutation or treatment with 15 μ M NA also do not affect the level of CDK9 or Cyclin T1 in whole-cell extract (Fig EV2F and G). NA treatment of wild-type HEK293 cells also has no effect on polyadenylation (Fig EV2H).

The effect of CDK9 inhibition on pol II CTD phosphorylation was analyzed by Western blotting of chromatin fractions (Fig 3A and B). As expected, CDK9as inhibition causes loss of Ser2P and Ser5P with two different phosphoantibodies to each CTD mark (ab5095 and ab5121 from Abcam, 13499S and 13523S from Cell Signaling) while NA treatment has no effect on CTD phosphorylation in wild-type HEK293 cells. ChIP-qPCR on *KPNB1* also indicates that CDK9as inhibition causes loss of Ser2P and Ser5P, whether ratioed to pol II or not (Fig 3C and Appendix Fig S2), indicating that *in vivo* CDK9 activity is necessary for efficient Ser2 and Ser5 phosphorylation.

These findings reinforce the conclusion that the effect of DRB on pol II is due to CDK9 inhibition.

CDK9 phosphorylates several transcription and splicing factors *in vivo*

Phosphorylation of several non-CTD CDK9 targets plays critical roles in gene expression (Sanso *et al*, 2016; Zaborowska *et al*, 2016; Decker *et al*, 2019). To identify the *in vivo* targets of CDK9, we performed biological replicates of SILAC phosphoproteomics in HeLa cells treated with DMSO or DRB for 30 min (Figs 4A and EV3A; Dataset EV1). We found 100 phosphosites across 74 proteins decreased more than 1.5-fold and with a *P*-value < 0.1. Among these phosphosites, 34 have a SP or a TP motif and are located in 25 different proteins (Fig EV3B). In line with previous similar studies, most CDK9 targets are factors involved in transcription, RNA processing, and RNA biology. Importantly, we identified several known targets of CDK9, including MED1 (T1440), MEPCE (T213, S217, T291), NELFA (S225), SPT5 (S666, S671), and SPT6 (T1523) (Sanso *et al*, 2016; Vos *et al*, 2018a, 2018b; Decker *et al*, 2019). We also identified several residues of the splicing factors SF3B1 (T142, T227, and T436) and CDC5L (T377, T396, T430, and T442) as targets of CDK9. However, there is only limited overlap with previously published CDK9 *in vitro* or *in vivo* phosphoproteomics (Fig EV3C; Sanso *et al*, 2016; Decker *et al*, 2019).

We have generated a new phosphoantibody for SF3B1 T142P, as SF3B1 is known to have functions in splicing and definition of the last exon (Kyburz *et al*, 2006; Tellier *et al*, 2020a). Kinase-phosphatase switches have recently been shown to regulate transcription at the 3' end of gene and CDK9 and PP1 activities play a

major role in controlling SPT5 T806 phosphorylation and pol II elongation close to poly(A) sites (Parua *et al*, 2018, 2020; Cortazar *et al*, 2019). In addition, PP2A is known to dephosphorylate SPT5 S666P (Parua *et al*, 2018, 2020; Huang *et al*, 2020). Accordingly, we analyzed the effect on transcription of low concentrations of three small molecule inhibitors, 25 nM Tautomycin (TT), which inhibits PP1, and 2.5 nM Calyculin A (CA) or 2.5 nM LB-100, which inhibits PP2A. H3S10P and Myc S62P, which are known targets of PP1 and PP2A, respectively, were used to control for specific inhibition (Appendix Fig S3A). We observed that at the concentrations used, TT preferentially inhibits PP1, while CA and LB-100 mainly inhibit PP2A.

Western blotting of the chromatin fraction of cells treated or not with CDK9 inhibitors confirms that CDK9 phosphorylates SF3B1 T142P while PP1, but not PP2A, dephosphorylates this phospho-residue (Figs 4B and EV3D).

These findings expand the repertoire of transcription and RNA processing factors phosphorylated by CDK9 and emphasize the important role that reversible protein phosphorylation plays in the regulation of transcription and cotranscriptional processes at the end of genes.

CDK9 inhibition promotes the loss of interaction of SF3B1 and CPA factors with pol II

The SF3B complex has been shown to interact with mRNA CPA factors to promote mRNA cleavage and polyadenylation (Kyburz *et al*, 2006). Accordingly, we investigated whether the loss of SF3B1 phosphorylation following CDK9 inhibition could result in a loss of interaction with CPA factors, which could in turn explain the loss of mRNA polyadenylation after CDK9 inhibition. SF3B1 immunoprecipitation from HeLa cells did not indicate that CPA factors strongly interact with SF3B1 (Dataset EV2). However, as it is possible that only a small proportion of SF3B1 interacts with CPA factors, we performed CPSF2 immunoprecipitation from the CDK9as cell line with or without NA treatment (Fig 4C). Interaction between CPSF2 and CPSF3, SF3B1, and SF3B3 was detected. Interestingly, the interaction between CPSF and SF3B proteins was not affected by NA treatment. However, the interaction between CPSF2 and pol II was markedly decreased by CDK9 inhibition. There is also decreased interaction between SF3B1 and pol II following CDK9 inhibition as shown by immunoprecipitation of SF3B1 from the CDK9as cell line with or without NA or DRB treatment (Fig 4D). Importantly, the interaction between SF3B1 and SF3B2 is not affected by NA or DRB treatment. These experiments suggest that the loss of SF3B1 from chromatin (Figs 4B and EV3E) is due to loss of interaction with pol II.

Thus, CDK9 inhibition decreases SF3B1 phosphorylation and its interaction with total pol II without affecting SF3B1 interaction with other SF3B proteins and CPA factors.

Figure 3. Inhibition of analog-sensitive (as) CDK9 has the same effect on elongation as small molecule CDK9 inhibitors.

- Western blot of total pol II, Ser2P (Abcam or Cell Signaling), Ser5P (Abcam or Cell Signaling), and histone H3 as a loading control, on the chromatin fraction of CDK9as or wild-type HEK293 cells treated with DMSO or 15 μ M 1-NA-PP1 for 15 or 30 min.
- Quantification of the western blots shown in A. *n* = 2 biological replicates, except for Ser2P / pol II (Abcam) CDK9as NA 30 min, Ser5P / pol II (Abcam) CDK9as NA 15 min and NA 30 min, and Ser5P / pol II (Cell Signaling) CDK9as NA 30 min, where *n* = 3 biological replicates.
- ChIP-qPCR of total pol II and of Ser2P (Abcam or Cell Signaling), and Ser5P (Abcam or Cell Signaling) ratioed to total pol II on *KPNB1*. *n* = 3 biological replicates, mean \pm SEM, *P*-value: **P* < 0.05, ***P* < 0.01, ****P* < 0.001. Statistical test: two-tailed unpaired *t* test.

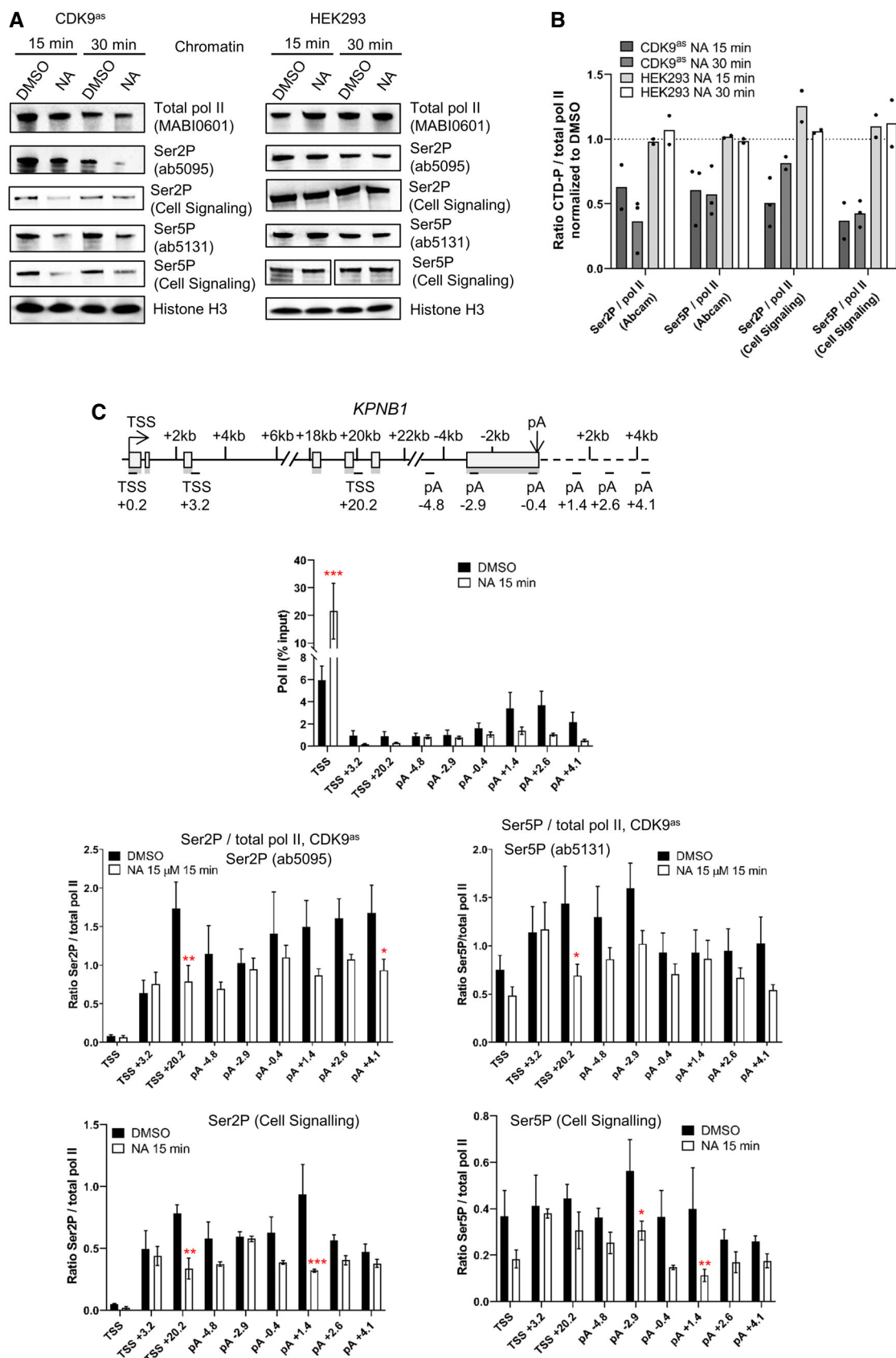


Figure 3.

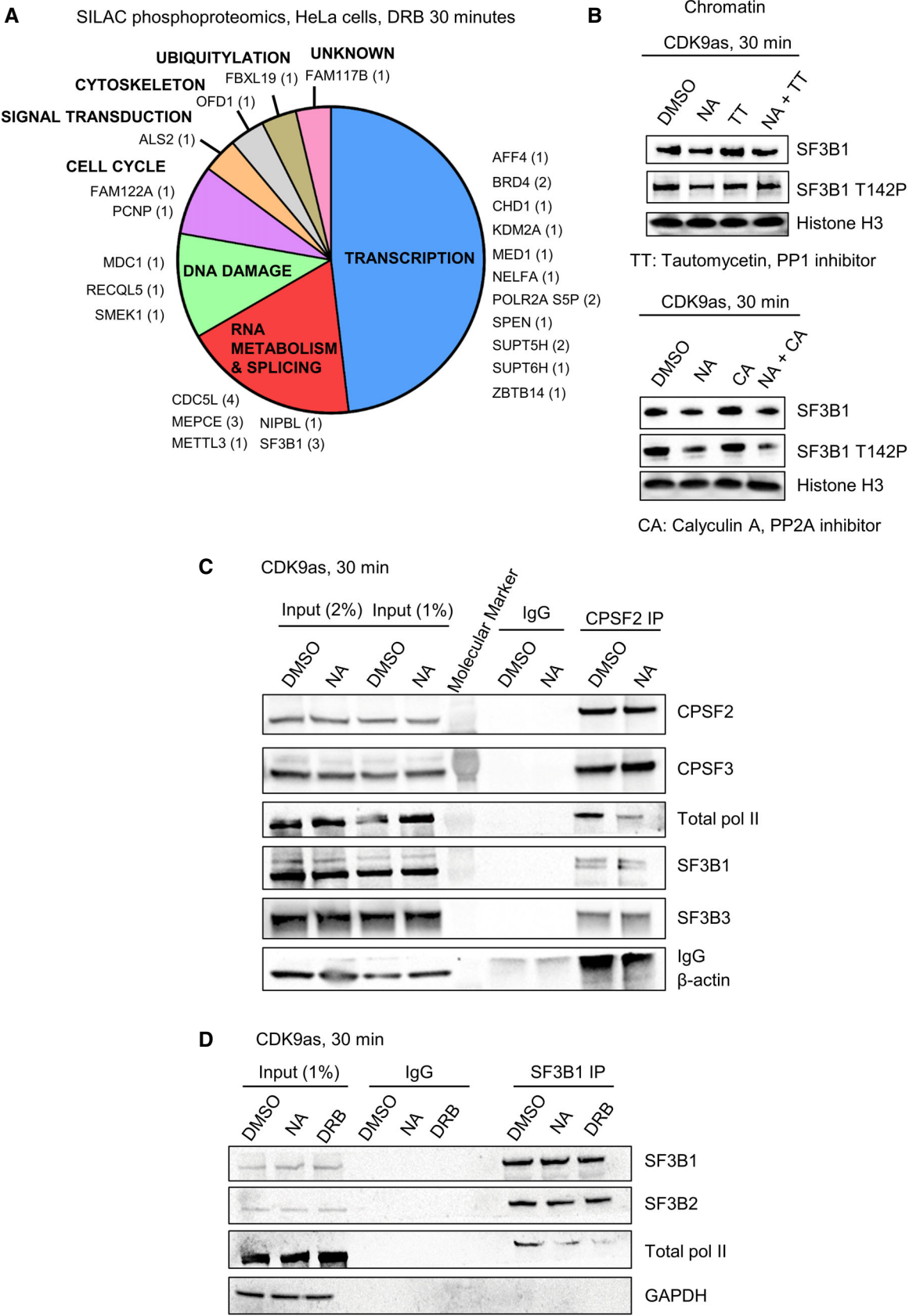


Figure 4.

Figure 4. CDK9 phosphorylates several transcription and splicing factors *in vivo* and CDK9 inhibition promotes the loss of interaction of SF3B1 and CPA factors with pol II.

- A Distribution of the proteins found to be phosphorylated by CDK9 in SILAC phosphoproteomics in HeLa cells treated or not with 100 μ M DRB for 30 min (fold change > 1.5 in both biological replicates, number of phosphopeptides decreased shown in brackets).
- B Western blot of total SF3B1, SF3B1 T142P, and histone H3 as a loading control, on the chromatin fraction of CDK9as cells treated for 30 min with DMSO, NA, tautomycin (TT), calyculin A (CA), NA + TT, or NA + CA. The histone H3 loading control (CA samples) is the same as the loading control shown in Appendix Fig S3B as the same Western blot experiment is shown in two different figs.
- C Co-immunoprecipitation of CPSF2 in the CDK9as cell treated for 30 min with DMSO or NA followed by Western blot with total pol II, CPSF2, CPSF3, SF3B1, SF3B3, and β -actin (negative control) antibodies.
- D Co-immunoprecipitation of SF3B1 in the CDK9as cell treated for 30 min with DMSO, NA, or DRB followed by Western blot with total pol II, SF3B1, SF3B2, and GAPDH (negative control) antibodies.

PP2A counteracts CDK9 activity at the 3' end of genes

As PP1 and PP2A reverse CDK9-mediated phosphorylation of several residues of SPT5 and SF3B1 (Fig 4B; Parua *et al*, 2018, 2020; Cortazar *et al*, 2019), the effect of PP1 and PP2A inhibition on pol II CTD Ser2 and Ser5 phosphorylation in the absence or presence of CDK9as inhibition was investigated (Appendix Fig S3B and C). As expected, NA causes loss of Ser2P and Ser5P while inhibition of PP1 with TT or PP2A with CA results in an increase of Ser2P and Ser5P, in line with the known roles of PP1 and PP2A as both CTD Ser2 and Ser5 phosphatases (Washington *et al*, 2002; Zheng *et al*, 2020; Vervoort *et al*, 2021). TT in addition to NA does not reverse the decrease in Ser2P and Ser5P levels seen in CDK9as cells, whereas CA in addition to NA causes an increase in Ser2P and Ser5P levels compared with NA alone, indicating that, for CTD phosphorylation, PP1 inhibition cannot overcome CDK9 inhibition, whereas PP2A inhibition can.

The effect of inhibition of these two phosphatases on transcription of the *KPNB1* gene was therefore investigated by pol II ChIP-qPCR (Fig 5A and Appendix Fig S4A). Inhibition of PP1 leads to an increase in pol II pausing at the TSS coupled to a termination defect downstream of the poly(A) site (primer TerDef), as previously reported (Eaton *et al*, 2020). Inhibition of PP2A by CA or LB-100 also results in increased pol II pausing at the TSS with apparent termination of pol II closer to the poly(A) site (CA, primer TerDef). Inhibition of CDK9 and PP1 at the same time has the same effect as CDK9 inhibition alone (Fig 5B). However, inhibition of PP2A and CDK9 at the same time mitigates the effect of CDK9 inhibition at the 3' end of the gene (see primer pA +1.4 for both DRB + CA and DRB + LB-100). Inhibition of CDK9 for 15 min followed by treatment with CA for another 15 min, or vice-versa, gives a similar outcome, although there is an increased level of pol II in the gene body when DRB is followed by CA (Appendix Fig S4B). A similar approach with TT results in the same outcome as DRB treatment alone (Appendix Fig S4C). Treatment of cells with DRB, CA, and TT together has the same effect as DRB and CA (Fig 5C).

To confirm our ChIP-qPCR results, we performed mouse spike-in total pol II ChIP-seq in HeLa cells treated for 30 min with DMSO, DRB, CA, or a combination of DRB and CA (Fig 6A–C). Inhibition of CDK9 by DRB causes an increase in pol II pausing, a loss of pol II entering productive elongation, an increase of the level of pol II across the last exon and premature termination. CA treatment results in a small increase in pol II pausing but does not affect pol II entry into productive elongation. Interestingly, inhibition of PP2A by CA promotes a specific increase in pol II across the last exon, indicating that both CDK9 and PP2A activities are required across

the last exon to ensure proper transcription elongation. Inhibition of both CDK9 and PP2A at the same time does not reverse the effect of CDK9 inhibition on pol II pausing downstream from the TSS and at the EEC but abrogates the effect of CDK9 inhibition on pol II transcription at the 3' end of protein-coding genes. Thus, the combination of CDK9 and PP2A inhibition results in pol II elongating further downstream of the poly(A) site than after CDK9 inhibition alone. This is noted on two single gene examples, *SUPT5H* and *WDR43* (Fig 6D).

These findings indicate that CDK9 and PP2A both play roles in regulating the progress of pol II at the 3' end of genes.

CDK9 and PP2A regulate mRNA cleavage and polyadenylation and alternative poly(A) site usage

As inhibition of PP2A abrogates the effect of CDK9 inhibition on transcription at the 3' end of the gene, we tested whether PP2A inhibition also reverses the effect of CDK9 inhibition on cleavage and polyadenylation. Treatment of cells for 30 min with DRB or DRB and CA followed by qRT-PCRs of newly synthesized nuclear polyadenylated mRNA from TNF α -induced genes indicates that inhibiting PP2A fully reverses the effect of CDK9 inhibition on the production of polyadenylated mRNA (Fig 7A and B). Surprisingly, inhibiting PP2A alone causes increased the production of polyadenylated mRNA for most of the genes tested, indicating that PP2A can act as a negative regulator of CPA. To confirm that CA does not block mRNA export, which could explain the increase in nuclear poly(A) + mRNAs, we carried out qRT-PCR on the cytoplasmic fraction (Fig 7C). CA treatment of cells also results in an increase in poly(A) + mRNAs in the cytoplasmic fraction, indicating that CA does not affect mRNA export. We confirmed these results with another PP2A inhibitor, LB-100 (Appendix Fig S5A–C). Inhibition of PP1 instead has little effect on polyadenylation of newly synthesized RNA (Appendix Fig S5D and E).

To determine whether CPA factor recruitment is affected by PP2A inhibition, we performed Western blots of Xrn2, CPSF2, and CPSF73 on the chromatin and nucleoplasm fractions following 30-min treatment with DRB, CA, or DRB and CA (Fig EV4A–C). Whereas CDK9 inhibition causes a decrease in Xrn2, CPSF2, and CPSF73 on chromatin, CA or DRB and CA treatment causes an increase in CPSF2 and CPSF73 recruitment to chromatin and a decrease of CPSF2 in the nucleoplasmic fraction. Importantly, there was no effect of DRB, CA, or DRB and CA on the total protein level of these termination factors in whole-cell extract (Fig EV4D). As pol II CTD Ser2P is associated with the

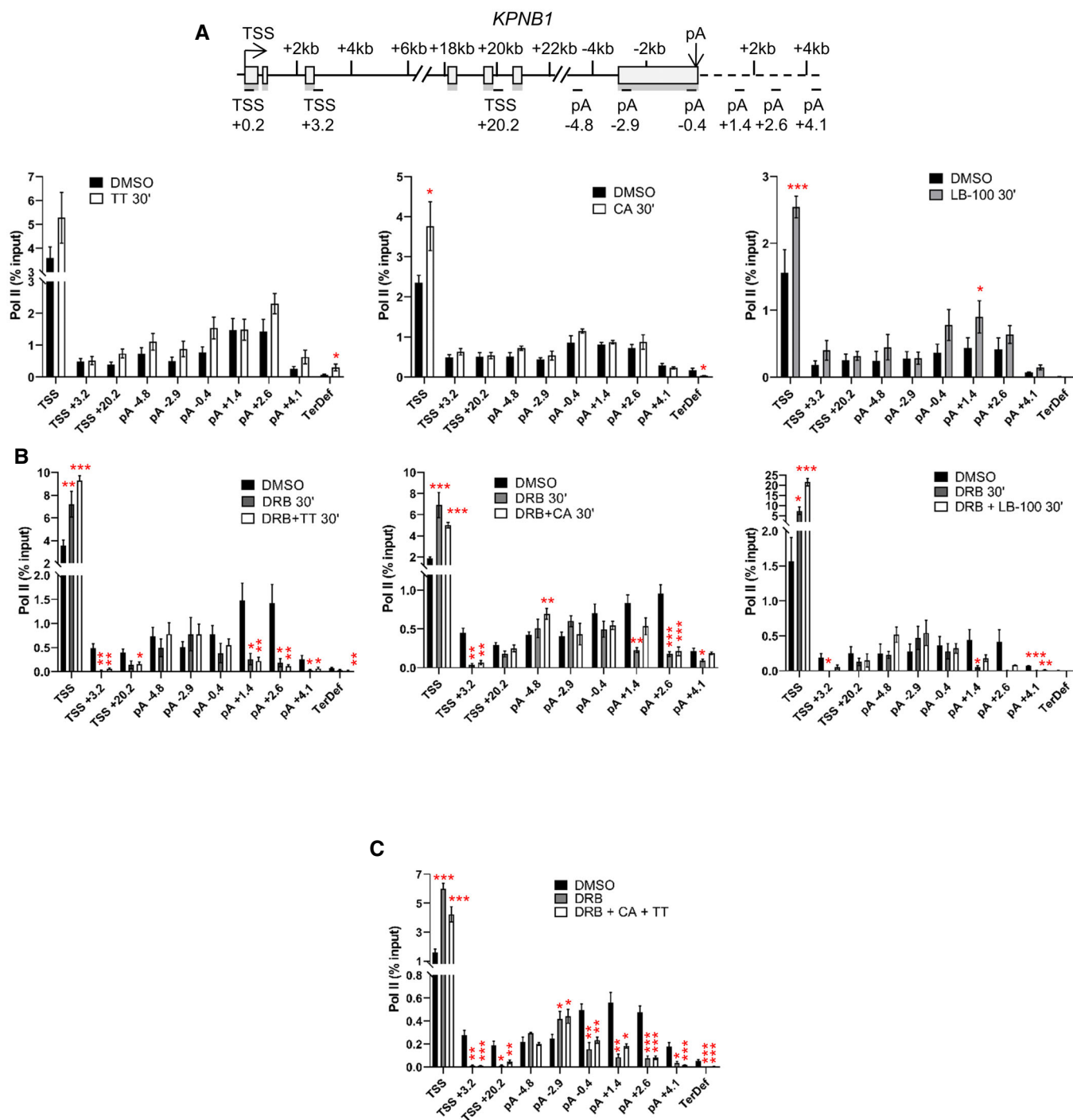


Figure 5. PP1 and PP2A regulate transcription of protein-coding genes.

A ChIP-qPCR of total pol II after 30-min treatment with DMSO, TT, CA, or LB-100 on *KPNB1*. $n = 3$ biological replicates, mean \pm SEM, P -value: $*P < 0.05$, $**P < 0.01$, $***P < 0.001$. Statistical test: two-tailed unpaired t -test.

B ChIP-qPCR of total pol II after 30-min treatment with DMSO, DRB, DRB + TT, DRB + CA, or DRB + LB-100 on *KPNB1*. $n = 3$ biological replicates, mean \pm SEM, P -value: $*P < 0.05$, $**P < 0.01$, $***P < 0.001$. Statistical test: two-tailed unpaired t -test.

C ChIP-qPCR of total pol II after 30-min treatment with DMSO or DRB + CA + TT on *KPNB1*. $n = 3$ biological replicates, mean \pm SEM, P -value: $*P < 0.05$, $**P < 0.01$, $***P < 0.001$. Statistical test: two-tailed unpaired t -test.

recruitment of CPA factors and CDK9 and PP2A modulate Ser2P, we investigated the effect of CDK9, PP2A or CDK9/PP2A inhibition on pol II, Ser2P, CPSF73, and CPSF2 levels by ChIP-qPCR on

the *KPNB1* gene. (Figs 7D and EV4E). DRB and CA treatment together results in a localized increase of the Ser2P/pol II ratio and an increased ratio of CPSF73/pol II and CPSF2/pol II at the

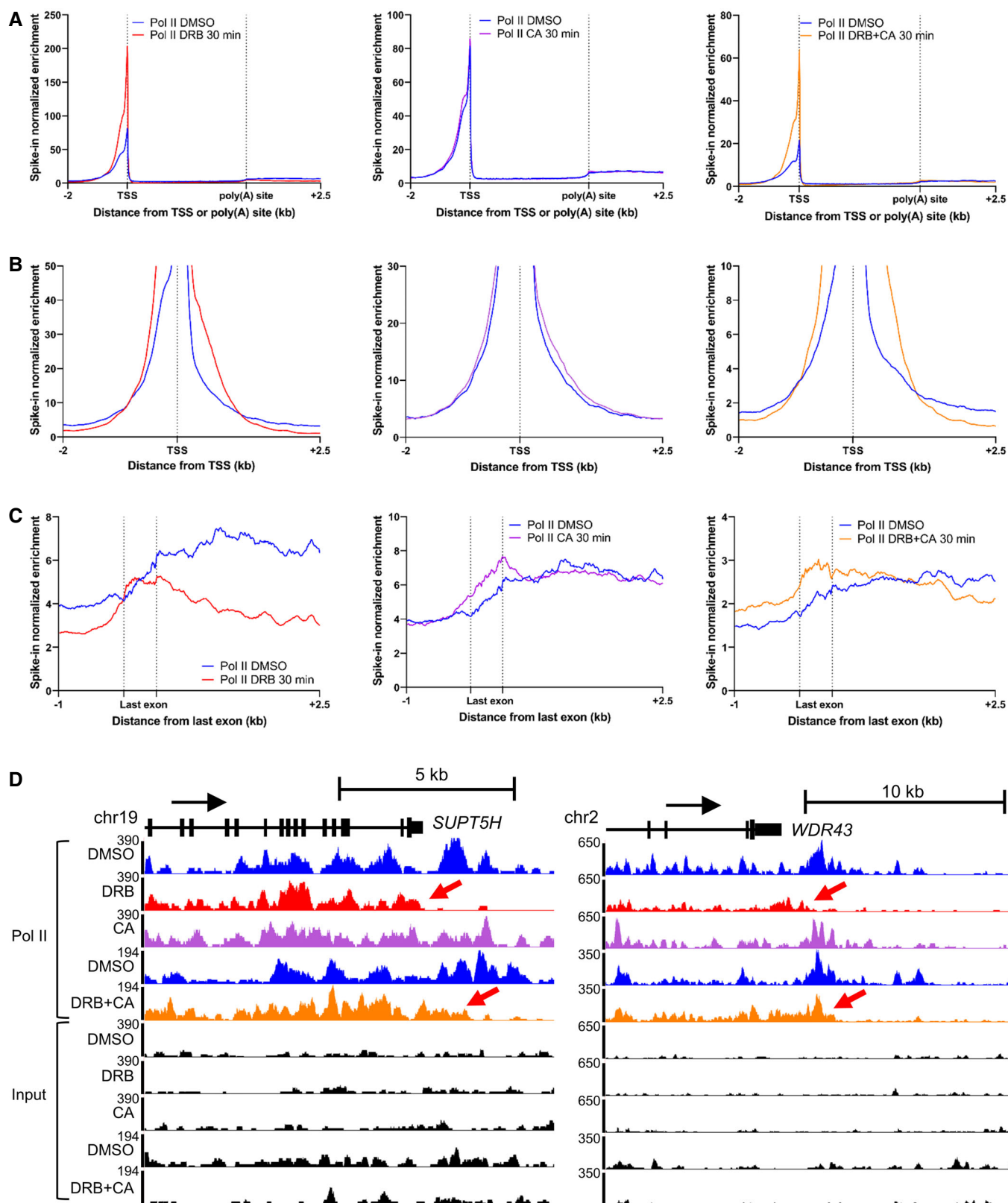


Figure 6.

Figure 6. PP2A counteracts CDK9 activity at the 3' end of genes.

- A Metagene profile of mouse spiked-in total pol II ChIP-seq in HeLa cells after 30-min treatment with DMSO (blue), DRB (red), CA (purple), or DRB and CA (orange) across scaled expressed protein-coding genes longer than 30 kb ($n = 3,490$).
- B Metagene profile of mouse spiked-in total pol II ChIP-seq in HeLa cells after 30-min treatment with DMSO (blue), DRB (red), CA (purple), or DRB and CA (orange) around the TSS. Only a part of the y-axis is presented to show the entry of pol II into productive elongation.
- C Metagene profile of mouse spiked-in total pol II ChIP-seq in HeLa cells after 30-min treatment with DMSO (blue), DRB (red), CA (purple), or DRB and CA (orange) around the scaled last exon of expressed genes longer than 40 kb ($n = 2,525$).
- D Screenshot of the genome browser of mouse spiked-in total pol II ChIP-seq tracks around the 3' end of the protein-coding genes *SUPT5H* and *WDR43*. Red arrows indicate premature termination of pol II (DRB tracks, red) and transcription further downstream the poly(A) site (DRB + CA tracks, orange).

3' end of *KPNB1*. Analysis of the nuclear polyadenylated *KPNB1* mRNA level indicates that, as expected from the 3'READS experiments, it is not induced by TNF α (Fig EV4F). However, the level of nuclear polyadenylated *KPNB1* mRNA increases after CA treatment while DRB and CA treatment at the same time leads to a modest increase in the poly(A) + mRNA level compared with DRB alone. In addition, DRB reduces Ser2P while CA or DRB and CA together do not. DRB treatment strongly decreases the interaction between pol II and SF3B1 and between pol II and CPSF2 and to a lesser extent between pol II and Xrn2 (Fig 7E). Interestingly, CA treatment alone increases the interaction between SF3B1 and pol II while the interaction between pol II and CPSF2 and Xrn2 is not affected. In contrast, the interaction between pol II and SF3B1 is still decreased after DRB and CA treatment while the interaction between pol II and CPSF2 and Xrn2 is unaffected, indicating that CDK9 and PP2A together regulate the interaction between pol II, SF3B1, and CPA complex components.

Further analysis of our 3'READS data indicates that 30 min of CDK9 inhibition has only a limited effect on intronic poly(A) site (IPA) usage, with only 4 genes exhibiting increased IPA and 3 genes exhibiting decreased IPA (Fig EV5A). In addition, 22 genes showed a shift toward proximal poly(A) site usage and 17 genes showed a shift toward distal poly(A) site usage following CDK9 inhibition (Fig EV5B). For three genes with a shift toward proximal poly(A) site usage after CDK9 inhibition in the 3'READS data, *EIF1*, *HCCS*, and *PCF11*, this was confirmed by qRT-PCR (Fig EV5C and D). PP2A inhibition promotes a shift toward distal poly(A) site usage on *EIF1* and *HCCS* (Fig EV5D). However, inhibiting both CDK9 and PP2A together reverses most of the effect of CDK9 inhibition on the three genes, with only *PCF11* still exhibiting some increase in proximal poly(A) site usage compared with the control.

These findings reinforce the role of the CDK9/PP2A kinase/phosphatase pair in regulating both poly(A) site function and transcription at the end of protein-coding genes.

Discussion

We previously showed that CDK9 inhibition, in addition to halting pol II at the EEC, leads to premature termination of pol II close to the poly(A) site (Laitem et al, 2015). We show here that premature termination of pol II is associated with loss of mRNA polyadenylation and loss of recruitment of polyadenylation and termination factors to chromatin. Although we have termed this 3' end CDK9 checkpoint the poly(A)-associated checkpoint, analysis of pol II transcription at single-nucleotide resolution using mNET-seq indicates that pol II slows down prematurely from the start of the last exon. Thus, CDK9 inhibition may be causing failure to properly define the last exon, which helps to ensure the correct transition of pol II between elongation and termination (Fig 8). In support of this, we identified several proteins involved in definition of the last exon and the transition between transcription elongation and termination, including SPT5, SF3B1, CDC5L, and the RNA m6a methyltransferase METTL3, (Kyburz et al, 2006; Ke et al, 2015; Cortazar et al, 2019; Parua et al, 2020; Tellier et al, 2020a) as targets of CDK9. CDK9 therefore joins other transcriptional CDKs, including CDK11 and CDK12, in the regulation of mRNA CPA, emphasizing the critical role of protein phosphorylation in this cotranscriptional process (Davidson et al, 2014; Eifler et al, 2015; Pak et al, 2015; Tellier et al, 2020b). Surprisingly, there is little overlap in targets between all the different CDK9 phosphoproteomic experiments published (Sanzo et al, 2016; Decker et al, 2019). This is likely explained by differences in the CDK9 inhibitors (DRB versus analog-sensitive cell line), *in vitro* vs *in vivo* approaches, and also different cell lines used (HeLa, Raji).

It has previously been shown that hyperactivation of P-TEFb via the degradation of the 7SK non-coding RNA, which negatively regulates P-TEFb activity, leads to global pol II readthrough at poly(A) sites (Castelo-Branco et al, 2013). This is in line with the demonstration that inhibition of PP1, which will mimic P-TEFb hyperactivation on, for example, SPT5 and the pol II CTD, also promotes

Figure 7. CDK9 and PP2A regulate mRNA cleavage and polyadenylation and alternative poly(A) site usage.

- A Schematic of the nuclear and cytoplasmic qRT-PCR experiments.
- B qRT-PCR of nuclear polyadenylated mRNAs of several TNF α induced or noninduced genes with a 30-min DMSO, DRB, CA, or DRB + CA treatment. $n = 6$ biological replicates, mean \pm SEM, P -value: * $P < 0.05$, ** $P < 0.01$, *** $P < 0.001$. Statistical test: two-tailed unpaired t -test.
- C qRT-PCR of cytoplasmic polyadenylated mRNAs of several TNF α induced or noninduced genes with a 30-min DMSO, DRB, CA, or DRB + CA treatment. $n = 4$ biological replicates, mean \pm SEM, P -value: * $P < 0.05$, ** $P < 0.01$, *** $P < 0.001$. Statistical test: two-tailed unpaired t -test.
- D ChIP-qPCR of Ser2P, CPSF73, or CPSF2 ratioed to total pol II after 30-min treatment with DMSO, DRB, CA, or DRB + CA on *KPNB1*. $n = 3$ biological replicates, mean \pm SEM, P -value: * $P < 0.05$, ** $P < 0.01$, *** $P < 0.001$. Statistical test: two-tailed unpaired t -test.
- E Co-immunoprecipitation of total pol II from HeLa cells treated for 30 min with DMSO, DRB, CA, or DRB + CA followed by Western blot with total pol II, Ser2P, SF3B1, CPSF2, Xrn2, and GAPDH antibodies.

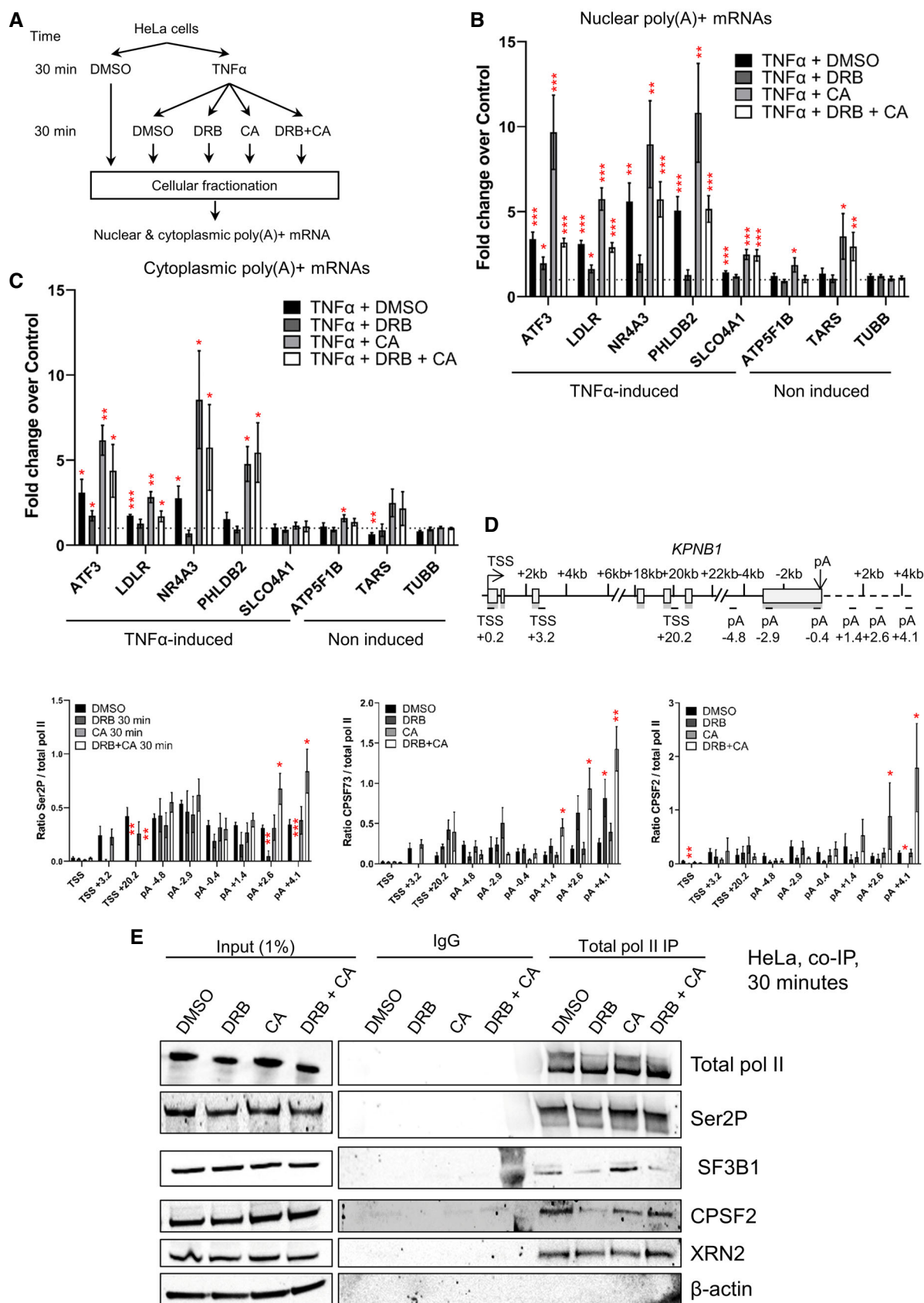


Figure 7.

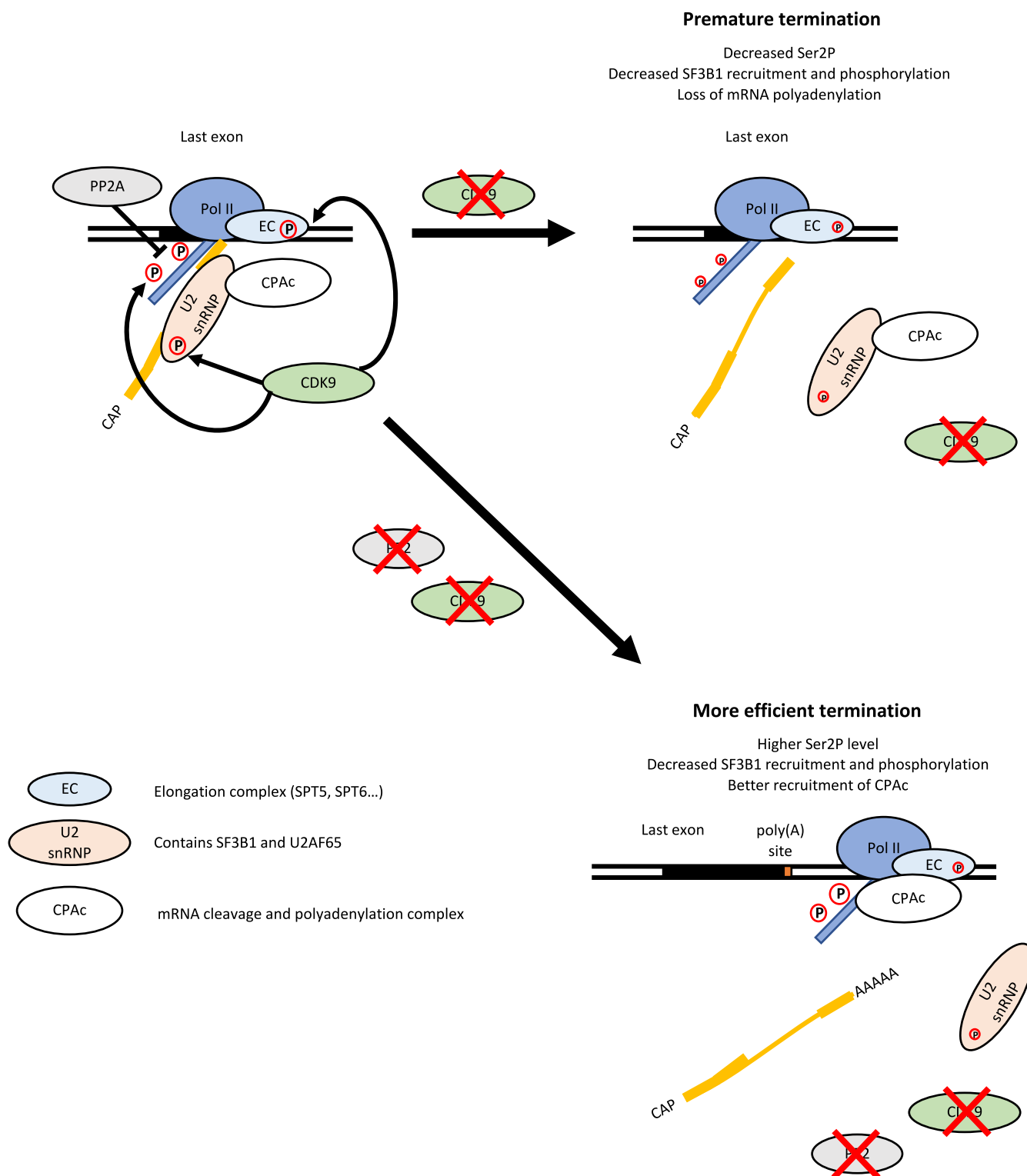


Figure 8. The role of CDK9 and PP2A in transcription termination and RNA maturation.

During the transcription cycle, CDK9 phosphorylates the pol II CTD on Ser2 and Ser5, proteins found in the elongation complex, for example, SPT5, and the SF3B1 subunit of the U2 snRNP. The phosphatase PP2A dephosphorylates the pol II CTD on Ser2P and Ser5P. CDK9 inhibition causes a decrease in pol II CTD phosphorylation and proteins found in the elongation complex and loss of the SF3B complex together with CPA factors from pol II, resulting in the premature termination of pol II and loss of polyadenylation. Inhibition of CDK9 and PP2A at the same time results in more phosphorylation of the pol II CTD, but not of SF3B1 T142P. However, PP2A inhibition counteracts the effect of CDK9 inhibition on transcription and mRNA CPA, likely via pol II CTD Ser2 phosphorylation, resulting in restored mRNA maturation and subsequent transcription termination.

transcriptional readthrough (Parua *et al*, 2018, 2020; Cortazar *et al*, 2019; Eaton *et al*, 2020). These results underline the importance of regulating PTEFb activity at the end of genes. However, knockout of 7SK does not result in global readthrough, (Bandiera *et al*, 2021; Studniarek *et al*, 2021) indicating that more work is required to understand the role this non-coding RNA plays in the process of transcription termination.

In line with previous findings, we found that CDK9 activity is needed for CTD phosphorylation on Ser2 and Ser5 *in vivo* (Czudnochowski *et al*, 2012; Ghamari *et al*, 2013; Laitem *et al*, 2015; Greifengberg *et al*, 2016). As Ser2 phosphorylation helps to recruit polyadenylation factors (Davidson *et al*, 2014; Eifler *et al*, 2015; Tellier *et al*, 2020b), loss of this mark would be expected to affect recruitment of polyadenylation factors. However, recruitment of the key polyadenylation factor, PCF11, which binds directly to Ser2P is not greatly affected (Laitem *et al*, 2015), raising the question of why the other polyadenylation factors are lost.

In addition to the previously demonstrated roles of PP1 and PP2A in transcription regulation, at the 5' and 3' ends of protein-coding genes, respectively (Cortazar *et al*, 2019; Eaton *et al*, 2020; Huang *et al*, 2020; Zheng *et al*, 2020; Vervoort *et al*, 2021), we found that inhibiting PP2A abrogates the premature termination caused by CDK9 inhibition. In addition, inhibition of PP2A reverses the loss of CTD phosphorylation and loss of CPA factors from chromatin caused by CDK9 inhibition, and production of polyadenylated mRNA is restored. The CDK9/PP2A kinase/phosphatase pair is therefore involved in regulating the recruitment and activity of the CPA complex. In contrast, inhibition of CDK9 and PP2A together does not reverse the loss of SF3B1 recruitment to the pol II caused by CDK9 inhibition, indicating that the role of CDK9 and PP2A in SF3B1 recruitment is more complex.

It has been previously shown that loss of the INTAC complex, which is composed of the PP2A core enzyme and the RNA endonuclease Integrator complex, reverses the effect of CDK9 inhibition at the EEC (Zheng *et al*, 2020; Fianu *et al*, 2021; Hu *et al*, 2021; Vervoort *et al*, 2021). Interestingly, we do not observe reversal of the effect of CDK9 inhibition at the EEC when PP2A is inhibited by Calyculin A or LB-100, suggesting that INTAC function at the EEC is independent of PP2A activity.

Although a low concentration of Tautomycin or Calyculin A can specifically inhibit PP1 or PP2A, respectively, we cannot rule out that these small molecule inhibitors affect other proteins. However, another PP2A inhibitor, LB-100 gave similar results. In addition, PP1 and PP2A are clearly not completely redundant as PP1, but not PP2A, dephosphorylates SF3B1 T142P. In addition, both phosphatases are active at the 5' and 3' ends of protein-coding genes but have different functions. PP1 inhibition leads to a termination defect, likely due to a high pol II elongation rate after the poly(A) site caused by hyperphosphorylation of SPT5, which impedes Xrn2-mediated transcription termination (Cortazar *et al*, 2019; Eaton *et al*, 2020). Conversely, PP2A inhibition seems to promote more efficient cleavage and polyadenylation of transcripts. We found that PP2A inhibition promotes better interaction between SF3B1 and total pol II while Ser2P and CPA factor recruitment to the pol II are the same as in untreated cells. A higher level of SF3B1 on the pol II complex may therefore improve the activity of the CPA complex rather than recruiting more CPA factors to the transcribing pol II.

Interestingly, in addition to phospho-SPT5, phospho-SF3B1 is a target of PP1, supporting a role for this phosphatase in splicing and potentially in the definition of the last exon (Mermoud *et al*, 1992; Shi *et al*, 2006). However, inhibition of PP1 does not reverse the loss of Ser2 and Ser5 phosphorylation caused by CDK9 inhibition. This result reinforces the notion that dephosphorylation of Ser2P and Ser5P by PP1 is redundant with other CTD phosphatases, including PP2A.

Our DRB mNET-seq time course indicates that after 5 min of CDK9 inhibition, the effect on pol II at the EEC is more drastic than at the 3' end of the genes, where a defect becomes clear only after 10-min inhibition. The drastic effect of CDK9 inhibition on mRNA CPA may indicate that the loss of mRNA polyadenylation precedes premature termination of pol II. Thus, dephosphorylation of CDK9 targets including the pol II CTD, SPT5, and SF3B1 and the loss of the CPA complex from chromatin would occur first. In support of this notion, the loss of CPA factors is stronger than the loss of pol II after 30 min of CDK9 inhibition (Figs 1F and 7D). The slowing down of pol II over the last exon and early disengagement of pol II may be caused by the subsequent loss of elongation factors, such as SPT5, SPT6, or the PAF1 complex in turn, as these keep pol II clamped onto the DNA template (Bernecky *et al*, 2017; Vos *et al*, 2018a; Hou *et al*, 2019). Loss of the CPA complex is likely linked to loss of pol II CTD phosphorylation, which helps to recruit CPA factors to pol II, and/or loss of an SF3B/CPA complex. Reversal of this by PP2A inhibition may be due to the increase in CTD/SF3B phosphorylation, which is followed by recovery of the normal pol II elongation rate/processivity and efficient cotranscriptional processes (pre-mRNA splicing and mRNA cleavage and polyadenylation). Currently, we cannot rule out any of these scenarios.

A decrease in the pol II level downstream of the poly(A) site can therefore be associated with premature nonproductive termination, where gene expression is aborted (CDK9 inhibition) or more efficient termination coupled to the production of mature polyadenylated mRNA (CDK9 and PP2A inhibition) (Fig 8). Premature termination of pol II caused by inhibition of CDK9 is associated with a decreased level of Ser2P and Ser5P and reduced recruitment of CPA factors. In contrast, inhibition of CDK9 and PP2A together promote more efficient termination of pol II with the production of *de novo* nuclear polyadenylated mRNA, which is associated with higher Ser2P, efficient recruitment of CPA factors, and termination closer to the poly(A) site.

Materials and Methods

Cell culture

HEK293 and HeLa cells were obtained from ATCC (ATCC® CRL-1573™ and ATCC® CCL-2™, respectively). HeLa, HEK293 parental cells, and CDK9as HEK293 cells were grown in DMEM medium supplemented with 10% fetal calf serum, 100 U/ml penicillin, 100 µg/ml streptomycin, 2 mM L-glutamine at 37°C and 5% CO₂. HEK293 and CDK9as cells were treated with 7.5, 10, or 15 µM 1-NA-PP1 (Cayman Chemical Company) for 15 and 30 min. HEK293, CDK9as, or HeLa cells were treated with 10 ng/ml of TNFα (PeproTech), 2.5 nM Calyculin A (Sigma), 25 nM Tautomycin (Bio-Techne), 2.5 nM LB-100 (Stratex Scientific Ltd), 100 µM DRB (Sigma) for 5,

10, 15, or 30 min. As a negative control, HEK293, CDK9as, and HeLa cells were treated with DMSO (the resuspension vehicle for NA, DRB, Calyculin A, LB-100, and Tautomycin). Cells were routinely checked to be free of mycoplasma contamination using Plasmato Test Mycoplasma Detection Kit (InvivoGen, rep-pt1).

Analog-sensitive cell line creation

Guide RNAs were computationally designed.

Guide RNA 1: 5'-GCTCGCAGAACTCGAACACC-3'.

Guide RNA 2: 5'-CTTCTGCGAGCATGACCTTGC-3'.

The modified CDK9 genomic sequence (NCBI RefSeq Accession NG_033942.1) (500 bp either site of the mutation) was cloned into pcDNA3 and used as the repair template for genome editing. The repair template contains a TTC (phenylalanine) to GCT (alanine) mutation. The guide (g)RNAs inserts were cloned into the pX462 vector (obtained from Addgene). HEK293 cells were transfected with the gRNA vectors and correction template using Lipofectamine 2000 (Life Technologies) following the manufacturer's instructions. Single clones were isolated by low-density plating after Puromycin and Neomycin selection. Genomic DNA from each clone was analyzed using PCR and Sanger sequencing.

gDNA preparation

HEK293 and CDK9as cells were incubated in 180 µl ChIP lysis buffer (10 mM Tris-HCl pH8.0, 0.25% Triton X-100, 10 mM EDTA) for 10 min and sonicated for 3 min (30 s on/30 s off) using a Q800R2 sonicator (QSONICA). 20 µl ammonium acetate was added (final concentration of 400 mM) and samples were mixed with 200 µl phenol/chloroform by vortexing. The samples were centrifuged at 13,000 g for 5 min at 25°C and the upper phase was transferred to a new tube. Genomic DNA was precipitated in 70% ethanol, pelleted by centrifugation at 13,000 g for 5 min at 25°C and dissolved in nuclease free water. A CDK9 fragment was PCR amplified using the following primers: Forward: 5'-AAGGCTTCTGAGACAGCTGG-3'; Reverse: 5'-CAACCAGCTTCTTCTTCTCCTGC-3'. DNA was purified using a QIAquick PCR purification kit (Qiagen) and sequenced by the Source Bioscience Sanger Sequencing Service, Oxford.

RNA preparation

RNA was extracted from HEK293 and CDK9as cells using a Quick-RNA Miniprep kit (Zymo Research) according to the manufacturer's instructions. Reverse-transcription (RT) was performed with 500 ng of RNA using random hexamers with the SuperScript III kit (Invitrogen) according to the manufacturer's instructions. Sequencing was performed on a cDNA PCR fragment generated with Forward primer: 5'-AAAGCAGTACGACTCGGTGG-3' and Reverse primer: 5'-GTAGAGGCCGTTAAGCAGCA-3', purified using a QIAquick PCR purification kit (Qiagen) and sequenced by the Source Bioscience Sanger Sequencing Service, Oxford.

Cell proliferation analysis

Cells were seeded at 500/well in 95 µl in 96-well microplates (Greiner, 655090) and measured every 12 or 24 h by adding alamarBlue HS (Invitrogen) (1/20) and reading in a fluorimeter after

1 h's incubation, according to the manufacturer's instructions. 1-NA-PP1 or DMSO was added to the cells as noted on the figure.

Chromatin immunoprecipitation (ChIP)

ChIP analysis were performed as previously described (Tellier *et al*, 2020b). HeLa, HEK293, and CDK9as cells were grown in 100 or 150 mm dishes until they reached ~80% confluence. The cells were fixed with 1% formaldehyde for 10 min at room temperature with shaking. Formaldehyde was quenched with 125 mM glycine for 5 min at room temperature with shaking. The cells were washed twice with ice-cold PBS, scraped with ice-cold PBS, and transferred into 1.5 or 15 ml Eppendorf tubes. Cells were pelleted for 5 min at 1,500 g at 4°C. The pellets were then resuspended in ChIP lysis buffer (10 mM Tris-HCl pH8.0, 0.25% Triton X-100, 10 mM EDTA, protease inhibitor cocktail, and phosphatase inhibitor) and incubated 10 min on ice before being centrifuged at 1,500 g for 5 min at 4°C. Pellets were resuspended in ChIP wash buffer (10 mM Tris-HCl pH8.0, 200 mM NaCl, 1 mM EDTA, protease inhibitor cocktail, and phosphatase inhibitor) and centrifuged at 1,500 g for 5 min at 4°C. Pellets were resuspended in ChIP sonication buffer (10 mM Tris-HCl pH 8.0, 100 mM NaCl, 1 mM EDTA, protease inhibitor cocktail, and phosphatase inhibitor) and incubated 10 min on ice. HeLa cells were sonicated for 30 cycles, 30 s on/30 s off using a Bioruptor Pico (Diagenode). HEK293 and CDK9as cells were sonicated for 1 h, 30 s on/30 s off, 40% amplitude, using a Q800R2 sonicator (QSONICA). Chromatin was pelleted at 15,800 g for 15 min at 4°C and supernatant transferred to a new Eppendorf tube.

Chromatin was precleared for 30 min on a rotating wheel at 4°C with 10 µl of Protein G Dynabeads, previously washed with 100 µl of RIPA buffer (10 mM Tris-HCl pH8.0, 150 mM NaCl, 1 mM EDTA, 0.1% SDS, 1% Triton X-100, 0.1% sodium deoxycholate). Chromatin was quantified on a NanoDrop One with 60–100 µg of chromatin used per IP (antibodies described in Appendix Table S1) and incubated overnight on a rotating wheel at 4°C. 15 µl of Dynabeads per IP were washed in 100 µl RIPA buffer. The beads were saturated with 15 µl RIPA containing 4 mg/ml of bovine serum albumin (BSA) and mixed overnight on a rotor at 4°C.

Dynabeads were then mixed for 1 h on a rotating wheel at 4°C with the chromatin incubated with the antibody. Beads were then washed three times with 300 µl ice-cold RIPA buffer, three times with 300 µl High Salt Wash buffer (10 mM Tris-HCl pH8.0, 500 mM NaCl, 1 mM EDTA, 0.1% SDS, 1% Triton X-100, 0.1% sodium deoxycholate), twice with 300 µl LiCl Wash buffer (10 mM Tris-HCl pH8.0, 250 mM LiCl, 1 mM EDTA, 1% NP-40, 1% sodium deoxycholate), and twice with 300 µl TE buffer (10 mM Tris-HCl pH 7.5, 1 mM EDTA). Each sample was eluted twice from the Dynabeads with 50 µl of Elution buffer (100 mM NaHCO₃, 1% SDS, 10 mM DTT) for 15 min at 25°C at 1,400 rpm on a Thermomixer. For each input sample, 90 µl of Elution buffer was added to 10 µl total input. Each sample was treated with RNase A (0.6 µl of 10 mg/ml) for 30 min at 37°C followed by the addition of 200 mM NaCl and a 5-h incubation at 65°C to reverse the cross-links. Precipitation was performed overnight at -20°C following the addition of 2.5x volume of 100% ethanol. Ethanol was removed after a 20-min centrifugation at 15,800 g at 4°C and pellets resuspended in 100 µl TE, 25 µl 5x Proteinase K buffer (50 mM Tris-HCl pH 7.5, 25 mM EDTA, 1.25% SDS) and 1.5 µl Proteinase K (20 mg/ml). The

samples were incubated 2 h at 45°C to degrade the proteins. DNA was purified using Qiagen PCR Purification Kit and kept at −20°C.

ChIP samples were analyzed by real-time qPCR using QuantiTect SYBR Green PCR kit (Qiagen) and Rotor-Gene RG-3000 (Corbett Research). Signals are presented as percentage of Input after removing the background signal from the IP with the IgG antibody. The sequence of primers used for ChIP-qPCR is given in Appendix Table S2. Experiments were replicated three times, and each ChIP sample was measured in triplicate by qPCR. A version of the protocol is maintained at protocols.io <https://protocols.io/view/chip-qpcr-in-human-cells-bxy2ppye.html>.

Mouse spike-in (BV2a cells) ChIP-seq of total pol II (Active Motif, 39,097) in HeLa cells treated with DMSO, 100 µM DRB, 2.5 nM CA, or 100 µM DRB + 2.5 nM CA were performed in biological duplicates. BV2a cells were processed as described before until obtaining sonicated chromatin. To each HeLa chromatin sample, 10% of mouse chromatin was added before the overnight immunoprecipitation. Seven total pol II IPs have been performed for each ChIP-seq condition. Preparation of ChIP-seq library was prepared with the NEBNext Ultra II DNA Library Prep Kit for Illumina (NEB), according to the manufacturer's instructions. DNA sequencing was conducted by the high-throughput genomics team of the Wellcome Trust Centre for Human Genetics (WTCHG), Oxford or by Novogene UK. A version of the protocol is maintained at protocols.io <https://protocols.io/view/chip-seq-in-human-cells-with-mouse-cells-spike-in-bxxwpppe.html>.

Co-immunoprecipitation

For each sample and IgG control: 120 µl of Dynabeads M-280 Sheep anti-mouse IgG (Thermo Fisher) or 40 µl of Dynabeads protein G (Thermo Fisher) were preblocked overnight at 4°C on a wheel at 16 rpm in 1 ml of PBS supplemented with 0.5% BSA. The next day, the beads were washed three times in IP buffer (25 mM Tris-HCl pH 8.0, 150 mM NaCl, 0.5% NP-40, 10% Glycerol, 2.5 mM MgCl₂), before being incubated for 2 h at 4°C on a wheel at 16 rpm in 600 µl of IP buffer supplemented with 5 µg of total pol II antibody (MAB10601, MBL International), 5 µg of SF3B1 antibody (D221-3, MBL International), 5 µg of CPSF2 antibody (A301-581A, Bethyl Laboratories), or Normal Rabbit IgG (2729S, Cell Signaling Technology) and protease inhibitor cocktail (cOmplete™, EDTA-free Protease Inhibitor Cocktail, Sigma-Aldrich). In the meantime, a 70–80% confluent 15 cm dish of HeLa cells was washed twice with ice-cold PBS and scrapped with ice-cold PBS supplemented with protease inhibitor cocktail. The cells were pelleted at 500 g for 5 min at 4°C. The pellets were resuspended in 800 µl of Lysis buffer (50 mM Tris-HCl pH 8.0, 150 mM NaCl, 1% NP-40, 10% glycerol, 2.5 mM MgCl₂, protease inhibitor cocktail, PhosSTOP (Sigma-Aldrich), 1× PMSF (Sigma-Aldrich), and 25–29 units of Benzonase (Merck Millipore)) and incubated at 4°C on a wheel at 16 rpm for 30 min. After centrifuging for 15 min at 13,000 g at 4°C, 800 µl of Dilution buffer (150 mM NaCl, 10% glycerol, 2.5 mM MgCl₂, protease inhibitor cocktail, PhosSTOP, and 1× PMSF) was added to each supernatant.

The beads conjugated with antibodies were washed three times with IP buffer supplemented with protease inhibitor cocktail before being incubated with 1 mg of proteins at 4°C on a wheel at 16 rpm for 2 h. The beads were washed three times with IP buffer supplemented with protease inhibitor cocktail and three times with IP

buffer without NP-40 supplemented with protease inhibitor cocktail. Proteins were eluted in 40 µl of 1× LDS plus 100 mM DTT for 10 min at 70°C. Western blots were performed with NuPAGE Novex 3–8% Tris-Acetate Protein Gels (Life Technologies). For the SF3B1 immunoprecipitation followed by proteomics, glycerol was removed from each buffer. A version of the protocol is maintained at protocols.io <https://protocols.io/view/co-immunoprecipitation-in-human-cells-bw8hpt6.html>.

Protein extraction and Western blot

Western blot analysis was performed on chromatin and nucleoplasm extracts as previously described in the mNET-seq procedure (Nojima *et al*, 2015). A ~80% confluent 15 cm dish was washed twice with ice-cold PBS and scrapped in 5 ml of ice-cold PBS. The cells were pelleted at 420 g for 5 min at 4°C. After discarding the supernatant, the cells were resuspended in 4 ml of ice-cold HLB + N buffer (10 mM Tris-HCl (pH 7.5), 10 mM NaCl, 2.5 mM MgCl₂ and 0.5% (vol/vol) NP-40) and incubated on ice for 5 min. The cell pellets were then underlayered with 1 ml of ice-cold HLB + NS buffer (10 mM Tris-HCl (pH 7.5), 10 mM NaCl, 2.5 mM MgCl₂, 0.5% (vol/vol) NP-40 and 10% (wt/vol) sucrose). Following centrifugation at 420 g for 5 min at 4°C, the nuclear pellets were resuspended by pipetting up and down in 125 µl of NUN1 buffer (20 mM Tris-HCl (pH 7.9), 75 mM NaCl, 0.5 mM EDTA and 50% (vol/vol) glycerol) and moved to a new 1.5 ml ice-cold microcentrifuge tube. Following the addition of 1.2 ml of ice-cold NUN2 buffer (20 mM HEPES-KOH (pH 7.6), 300 mM NaCl, 0.2 mM EDTA, 7.5 mM MgCl₂, 1% (vol/vol) NP-40 and 1 M urea), the tubes were vortexed at maximum speed for 10 s and incubated on ice for 15 min with a vortexing step of 10 s every 3 min. The samples were centrifuged at 16,000 g for 10 min at 4°C and the supernatant kept as the nucleoplasmic fractions while the chromatin pellets were washed with 500 µl of ice-cold PBS and then with 100 µl of ice-cold water. The chromatin pellet was then digested in 100 µl of water supplemented with 1 µl of Benzonase (25–29 units, Merck Millipore) for 15 min at 37°C in a thermomixer at 1,400 rpm. 10 µg of proteins was boiled in 1× LDS plus 100 mM DTT. Western blots were performed with NuPAGE Novex 4–12% Bis-Tris Protein Gels (Life Technologies).

For whole-cell extract, cells were washed in ice-cold PBS twice, collected in ice-cold PBS with a 800 g centrifugation for 5 min at 4°C. The pellets were resuspended in RIPA buffer supplemented with protease inhibitor cocktail and PhosSTOP, kept on ice for 30 min with a vortexing step every 10 min. After centrifugation at 14,000 g for 15 min at 4°C, the supernatants were kept and quantified with the Bradford method. A 20 µg of proteins was boiled in 1× LDS plus 100 mM DTT. Western blots were performed with NuPAGE Novex 4–12% Bis-Tris Protein Gels (Life Technologies). The list of primary antibodies is shown in Appendix Table S1.

Secondary antibodies were purchased from Merck Millipore (Goat Anti-Rabbit IgG Antibody, HRP-conjugate, 12–348, and Goat Anti-Mouse IgG Antibody, HRP conjugate, 12–349), the chemiluminescent substrate (SuperSignal West Pico PLUS) from Thermo Fisher, and the membranes visualized on an iBright FL1000 Imaging System (Thermo Fisher). Quantification of the western blots was performed with Image Studio Lite software.

RNA subcellular fractionation

RNA subcellular fractionation as performed as described before (Neve *et al.*, 2016). A ~ 80% confluent 10 or 15 cm dish was washed twice with ice-cold PBS and scrapped in ice-cold PBS. The cells were pelleted at 100 g for 5 min at 4°C and then resuspended with slow pipetting in 1 ml of Lysis Buffer B (10 mM Tris-HCl pH 8, 140 mM NaCl, 1.5 mM MgCl₂, 0.5% NP-40). Following centrifugation at 1,000 g for 3 min at 4°C, 500 µl of the supernatant was moved to a new tube, centrifuged at 10,000 g for 1 min at 4°C, and the supernatant moved to a new tube as the purified cytoplasmic fraction. The pellets were resuspended in 1 ml of Lysis Buffer B and 100 µl of the Detergent Stock Solution (3.3% (w/v) sodium deoxycholate, 6.6% (v/v) Tween 40) was added under slow vortexing. Following a 5-min incubation on ice, the nuclei were spun down at 1,000 g for 3 min at 4°C. The nuclei pellet was then washed once more in 1 ml of Lysis Buffer B and spun down at 1,000 g for 3 min at 4°C. The nuclei pellet was resuspended in 1 ml of TRIzol using a 21-gauge syringe while 500 µl of TRIzol was added to the cytoplasmic fraction and incubated 5 min at room temperature. Following the addition of 100 µl or 200 µl of chloroform to the cytoplasmic or nuclear fraction, respectively, the samples were vortexed vigorously for 15 s and spun at 12,000 g for 15 min at 4°C. The aqueous fraction was transferred to a new tube containing 580 µl (nuclear) or 750 µl (cytoplasmic) of isopropanol. After a 10-min incubation at room temperature, the samples were spun at 12,000 g for 10 min at 4°C. The pellets were resuspended in 87 µl of water, 10 µl of 10 X DNase buffer, 2 µl of DNase I (Roche), and 1 µl of RNase OUT (ThermoFisher Scientific), and incubated 30 min at 32°C. RNA were then purified twice with phenol:chloroform pH 4.5 extraction, precipitated overnight in ethanol, and finally resuspended in nuclease free water and concentrations determined using a NanoDrop One. A version of the protocol is maintained at protocols.io <https://protocols.io/view/nuclear-rna-purification-byfhptj6.html>.

qRT-PCR

For each qRT-PCR reaction, 500 ng of RNA were reverse-transcribed with Oligo(dT)12–18 Primer (ThermoFisher Scientific) and the SuperScript III kit (ThermoFisher Scientific), according to the manufacturer's instructions. cDNA was amplified by qPCR with a QuantiTect SYBR Green PCR kit (QIAGEN) and a Rotor-Gene RG-3000 (Corbett Research). The sequence of primers used for qRT-PCR is given in Appendix Table S2. Values are normalized to GAPDH mRNA, used as control. Experiments were replicated at least three times to ensure reproducibility, and each RNA sample was measured in triplicate by qPCR.

3'READS protocol

The 3'READS protocol was originally described in (Hoque *et al.*, 2013). Briefly, 25–30 µg of RNA was subjected to one round of poly (A) selection using the Poly(A)Purist™ MAG kit (Ambion) according to the manufacturer's protocol, followed by fragmentation using Ambion's RNA fragmentation kit at 70°C for 5 min. Poly(A)-containing RNA fragments were isolated using the CU5T45 oligo (a chimeric oligo containing 5 Us and 45 Ts, Sigma) which were bound to the MyOne streptavidin C1 beads (Invitrogen) through biotin at

its 5' end. Binding of RNA with CU5T45 oligo-coated beads was carried out at room temperature for 1 h in 1x binding buffer (10 mM Tris-HCl pH 7.5, 150 mM NaCl, 1 mM EDTA), followed by washing with a low salt buffer (10 mM Tris-HCl pH 7.5, 1 mM NaCl, 1 mM EDTA, 10% formamide). RNA bound to the CU5T45 oligo was digested with RNase H (5 U in 50 µl reaction volume) at 37°C for 1 h, which also eluted RNA from the beads. Eluted RNA fragments were purified by phenol:chloroform extraction and ethanol precipitation, followed by phosphorylation of the 5' end with T4 kinase (NEB). Phosphorylated RNA was then purified by the RNeasy kit (Qiagen) and was sequentially ligated to a 5'-adenylated 3'-adapter (5'-rApp/NNNNGATCGTCCGACTGTAGAACTCTGAAC/3ddC) with the truncated T4 RNA ligase II (Bioo Scientific) and to a 5' adapter (5'-GUUCAGAGUUCUACAGUCCGACG AUC) with T4 RNA ligase I (NEB). The resultant RNA was reverse-transcribed to cDNA with Superscript III (Invitrogen) followed by a library preparation with the NEBNext Fast DNA Library Prep Set for Ion Torrent (NEB). cDNA libraries were sequenced on an Ion Torrent Proton.

mNET-seq and library preparation

mNET-seq was carried out as previously described (Nojima *et al.*, 2015) with minor changes. In brief, the chromatin fraction was isolated from four ~ 80% confluent 15 cm dish cells treated with DMSO or DRB (5, 10, 15, or 30 min). Chromatin was digested in 100 µl of MNase (40 units/µl) reaction buffer for 2 min at 1,400 rpm at 37°C in a Thermomixer. MNase was inactivated by the addition of 10 µl EGTA (25 mM). The soluble digested chromatin was collected after centrifugation at 15,800 g for 5 min at 4°C. The supernatant was diluted with 400 µl of NET-2 buffer and antibody-conjugated Dynabeads M-280 Sheep anti-mouse IgG (ThermoFisher Scientific) beads were added. Antibodies used are follows: Pol II (MAB10601, MBL International) and Ser5P (MAB10603, MBL International). Immunoprecipitation was performed at 4°C for 1 h. The beads were washed in the cold room six times with 1 ml of NET-2 buffer, and once with 100 µl of 1xPNKT (1xPNK buffer and 0.05% Triton X-100) buffer. Washed beads were incubated in 200 µl PNK reaction mix at 1,400 rpm at 37°C in a Thermomixer for 6 min. After the reaction, beads were washed once with 1 ml of NET-2 buffer and RNA was extracted with Trizol reagent. RNA was suspended in urea Dye and resolved on 6% TBU gel (ThermoFisher Scientific) at 200 V for 5 min. To size select 35–100 nt RNAs, a gel fragment was cut between BPB and XC dye markers. A 0.5-ml tube was prepared with 3–4 small holes made with 25G needle and placed in a 1.5-ml tube. Gel fragments were placed in the layered tube and broken down by centrifugation at 13,500 g for 1 min at room temperature. The small RNAs were eluted from the gel using RNA elution buffer (1 M NaOAc and 1 mM EDTA) at 25°C for 1 h on a rotating wheel at 16 rpm at room temperature. Eluted RNA was purified with SpinX column (Coster) with two glass filters (Milipore) and the flow-through RNA was ethanol precipitated. RNA libraries were prepared according to manual of TruSeq Small RNA Library Preparation Kit (Illumina). 12–14 cycles of PCR were used to amplify the library. Libraries were resolved on a 6% TBE polyacrylamide gel (ThermoFisher Scientific), size-selected to remove primer-primer ligated DNA, and eluted from the gel with the RNA elution buffer. Deep sequencing (HiSeq4000, Illumina) was

conducted by the high-throughput genomics team of the Wellcome Trust Centre for Human Genetics (WTCHG), Oxford.

SF3B1 proteomics

Sample processing protocol

SF3B1 duplicate pull-down samples were either digested in-solution after glycine elution at pH 2.3 and neutralization, or digested on-beads. On-beads and in-solution protein samples were, respectively, denatured with 8 M or 4 M urea in ammonium bicarbonate buffer (100 mM) for 10 min at room temperature. After denaturation, cysteines were reduced with of TCEP (10 mM) for 30 min at room temperature and alkylated with 2-Chloroacetamide (50 mM) for 30 min at room temperature in the dark. Samples were then predigested with LysC (1 µg/100 µg of sample) for 2 h at 37°C. Before overnight digestion with trypsin (1 µg/40 µg of sample) at 37°C, urea was diluted down to 2 M in ammonium bicarbonate buffer (100 mM) and calcium chloride was added at 2 mM final. The next day, tryptic digestion was stopped with the addition of formic acid (5%). Digested peptides were centrifuged for 30 min at 16,000 g at 4°C to remove undigested material. Supernatant was loaded onto hand-made C18 stage tip, pre-activated with 100% acetonitrile, by centrifugation at 1,500 g at room temperature. Peptides were washed twice in TFA 0.1%, eluted in 50% acetonitrile / 0.1% TFA and speed-vacuum dried. Peptides were resuspended into 2% acetonitrile / 0.1% formic acid before LC-MS/MS analysis. Peptides were separated by nano liquid chromatography (Thermo Scientific Easy-nLC 1,000) coupled in line a Q Exactive mass spectrometer equipped with an Easy-Spray source (Thermo Fischer Scientific). Peptides were trapped onto a C18 PepMac100 precolumn (300 µm i.d. x 5 mm, 100 Å, ThermoFischer Scientific) using Solvent A (0.1% Formic acid, HPLC grade water). The peptides were further separated onto an Easy-Spray RSLC C18 column (75 µm i.d., 50 cm length, Thermo Fischer Scientific) using a 60 min linear gradient (15% to 35% solvent B (0.1% formic acid in acetonitrile)) at a flow rate 200 nl/min. The raw data were acquired on the mass spectrometer in a data-dependent acquisition mode (DDA). Full-scan MS spectra were acquired in the Orbitrap (Scan range 350-1,500 m/z, resolution 70,000; AGC target, 3e6, maximum injection time, 100 ms). The 10 most intense peaks were selected for higher-energy collision dissociation (HCD) fragmentation at 30% of normalized collision energy. HCD spectra were acquired in the Orbitrap at resolution 17,500, AGC target 5e4, maximum injection time 120 ms with fixed mass at 180 m/z. Charge exclusion was selected for unassigned and 1+ ions. The dynamic exclusion was set to 20 s.

Data processing protocol

Tandem mass spectra were searched using Sequest HT in Proteome discoverer software version 1.4 against a protein sequence database containing 20,405 protein entries, including 20,122 Homo sapiens proteins (Uniprot database release of 2020-04) and 283 common contaminants. During database searching, cysteines (C) were considered to be fully carbamidomethylated (+57,0215, statically added), methionine (M) to be fully oxidized (+159,949, dynamically added), all N-terminal residues to be acetylated (+42,0106, dynamically added). Two missed cleavages were permitted. Peptide mass tolerance was set at 50 ppm on the precursor and 0.6 Da on the fragment ions. Data was filtered at FDR below 1% at PSM level.

SILAC phosphoproteomics

SILAC phosphoproteomics was performed as previously described (Poss *et al*, 2016). For stable isotope labelling with amino acids in cell culture (SILAC), HeLa cells were grown in DMEM media for SILAC (minus L-Lysine and L-Arginine, Fisher Scientific) and with SILAC dialysed fetal bovine serum (Dundee Cell Products). The medium was supplemented with either Arg10 (33.6 mg/ml) and Lys8 (73 mg/ml) or Arg0 and Lys0 for heavy and light treatment, respectively. After six passages at 1:3 ratio, SILAC incorporation test in HeLa cells was validated by mass spectrometry analysis.

Cells were passaged 7–8 times in SILAC media on 15 cm dishes. For each replicate, approximately 20 mg total protein was harvested for analysis after treatment with either DMSO or DRB for 30 min (first replicate: heavy cells DRB; light cells: DMSO; second replicate: heavy cells DMSO; light cells: DRB). After removing the media, each dish was scraped in 750 µl 95°C SDT (4% SDS, 100 mM Tris pH 7.9, 10 mM TCEP) buffer with subsequent heating at 95°C for 10 min. Lysates were sonicated for 2 min each. Protein concentrations were determined using a Bradford assay and samples were mixed 1:1 based on total protein concentrations. FASP was carried out in two 10 kDa MWCO filters with a 50 mM iodoacetamide alkylation step and proteins were digested in 2 M urea with 2% wt/wt Lys-C (Wako) for 6 h and 2% modified trypsin (Promega) for 12 h at 37°C. FASP eluates were acidified and desalted on Oasis HLB extraction cartridges.

TiO₂ phosphopeptide enrichment, ERLIC chromatography, and LC-MS/MS

Protocols were carried out as described (Stuart *et al*, 2015). An Orbitrap Velos (Thermo Fisher) was used for quantitative proteome analysis while an Orbitrap LTQ (Thermo Fisher) was used for phosphoproteomics. The samples were run on a 60-min gradient / 10 HCD method.

Proteomics data analysis

All raw mass spectrometry files for phosphoproteomics and quantitative proteomics were searched using the MaxQuant (v1.5.0.35) software package. Duplicate proteomic and phosphoproteomic were searched individually against the Uniprot human proteome database (downloaded on 16/01/2013) using the following MaxQuant parameters: multiplicity was set to 2 (heavy/light) with Arg10 and Lys8 selected, LysC/P was selected as an additional enzyme, “re-quantify” was unchecked, and Phospho (STY) was selected as a variable modification in both runs.

For phosphosite analysis, the Phospho (STY) table was processed with Perseus (v1.6.2.3) using the following workflow: Reverse and contaminant reads were removed, the site table was expanded to accommodate differentially phosphorylated peptides, and rows without any quantification were removed after site table expansion. Normalized heavy-to-light ratios were log2 transformed for statistical analyses. Differential abundance of peptides following DRB treatment was estimated by *t*-tests with Welch correction, two sided, unpaired. The volcano plot was prepared with GraphPad Prism 9.1. Sequence motif plots were prepared with WebLogo 3 (Crooks *et al*, 2004).

Generation of phosphoantibodies

Rabbit phosphoantibody against SF3B1 T142P was generated by Eurogentec based on the peptide sequence: H - CAD GKG T(PO3H2) PD PKM N - NH2 for SF3B1. Phosphoantibody specificity was ensured by selecting against recognition of the unphosphorylated peptide.

Quantification and statistical analysis

Gene annotation

The Gencode V35 annotation, based on the hg38 version of the human genome, was used to extract the list of protein-coding genes. A list of 9,883 expressed protein-coding genes was obtained by keeping only the genes longer than 2 kb and with their highest transcript isoform expressed in two nuclear RNA-seq in HeLa cells (Nojima *et al*, 2018) at more than 0.1 transcript per million (TPM), following quantification of transcript expression with Salmon version 0.14.1 (Patro *et al*, 2017). The list of used exons was obtained by extracting the location of exons from Gencode V35 from the highest transcribed nuclear poly(A) + RNA of each of the 9,883 protein-coding genes.

mNET-seq data processing

Adapters were trimmed with Cutadapt version 1.18 (Martin, 2011) in paired-end mode with the following options: --minimum-length 10 -q 15,10 -j 16 -A GATCGTCGGACTGTAGAACTCTGAAC -a AGATCGGAAGAGCACACGTCTGAACTCCAGTCAC. Trimmed reads were mapped to the human GRCh38.p13 reference sequence with STAR version 2.7.3a (Dobin *et al*, 2013) and the parameters: --runThreadN 16 --readFilesCommand gunzip -c -k --limitBAMsortRAM 20,000,000,000 --outSAMtype BAM SortedByCoordinate. SAMtools version 1.9 (Li *et al*, 2009) was used to retain the properly paired and mapped reads (-f 3). A custom python script (Nojima *et al*, 2015) was used to obtain the 3' nucleotide of the second read and the strandedness of the first read. Strand-specific bam files were generated with SAMtools. Samples normalization was checked against the termination region of the RNU2 snRNA, which is known to be insensitive to DRB (Medlin *et al*, 2003), and also verified for consistency against a previously published GRO-seq performed by our group in HeLa cells treated for 30 min with DMSO or DRB (Laitem *et al*, 2015). FPKM-normalized bigwig files were created with deepTools version 3.4.2 (Ramirez *et al*, 2016) bamCoverage tool with the parameters -bs 1 -p max --normalizeUsing RPKM.

Spike-in ChIP-seq processing

Adapters were trimmed with Cutadapt with the following options: --minimum-length 10 -q 15, 10 -j 16 -a AGATCGGAAGAGCA-CACGCTGAACTCCAGTCA. Trimmed reads were mapped to the human GRCh38.p13 and to the mouse GRCh38 reference genomes with STAR and the parameters: --runThreadN 16 --readFilesCommand gunzip -c -k --alignIntronMax 1 --limitBAMsortRAM 20000000000 --outSAMtype BAM SortedByCoordinate. SAMtools was used to retain the properly mapped reads and to remove PCR duplicates. Reads mapping to the DAC Exclusion List Regions (accession: ENCSR636HFF) were removed with BEDtools version 2.29.2 (Quinlan & Hall, 2010). SAMtools view with the -s option was used to subsample all the bam files to the bam file containing

the lowest number of reads. The normalization factor was then calculated as: (number of mouse reads) / (number of mouse + number of human reads) and applied to the generation of the bigwig files with deepTools bamCoverage tool with the parameters -bs 10 -p max -e --scaleFactor.

Analysis of 3' READS data

The analysis was performed exactly as in (Neve *et al*, 2016). Briefly, raw reads were mapped to the human genome (hg19) with Bowtie 2 (Langmead & Salzberg, 2012) using the option "-M 8 --local". Reads that were shorter than 15 nt, were nonuniquely mapped to genome (MAPQ < 10), or contained more than two mismatches in alignment were discarded. FPKM-normalized bigwig files were created with deepTools bamCoverage tool with the parameters -bs 10 -p max --normalizeUsing RPKM.

Metagene profiles

Metagene profiles of genes scaled to the same length were then generated with Deeptools2 computeMatrix tool with a bin size of 10 bp and the plotting data obtained with plotProfile --outFileNameData tool. Graphs representing the (IP / Input) signal (ChIP-seq) or the mNET-seq signal were then created with GraphPad Prism 9.1. Metagene profiles are shown as the average of two biological replicates.

P-values and significance tests

P-values were computed with an unpaired two-tailed Student's *t*-test. Statistical tests were performed in GraphPad Prism 9.1.

Data availability

Sequencing data have been deposited in GEO under accession code GSE176541 (<http://www.ncbi.nlm.nih.gov/geo/query/acc.cgi?acc=GSE176541>). The mass spectrometry proteomics data have been deposited to the ProteomeXchange Consortium via the PRIDE (Perez-Riverol *et al*, 2019) partner repository with the dataset identifier PXD026720 (SILAC) (<http://www.ebi.ac.uk/pride/archive/projects/PXD026720>) and PXD033694 (SF3B1) (<http://www.ebi.ac.uk/pride/archive/projects/PXD033694>). All data generated or analyzed during this study are included in the manuscript and supporting files. We include full excel spreadsheets representing original mass spectrometry data.

Expanded View for this article is available online.

Acknowledgments

We thank Chris Norbury for helpful comments on the manuscript. We thank Shabaz Mohammed for help with the SILAC phosphoproteomics. We thank the High-Throughput Genomics Group at the Wellcome Trust Centre for Human Genetics for sequencing. This work was supported by a Wellcome Trust Investigator Award (WT106134AIA and WT210641/Z/18/Z) and a Biotechnology and Biological Sciences Research Council grant (BB/R016836/1) to SM. AF's research is funded by the Biotechnology and Biological Sciences Research Council (BB/N001184/1) and JN is funded by an MRC studentship.

Author contributions

Michael Tellier: Conceptualization; data curation; formal analysis; validation; investigation; visualization; writing – original draft; writing – review and

editing. **Justyna Zaborowska:** Investigation. **Jonathan Neve:** Investigation. **Takayuki Nojima:** Investigation. **Svenja Hester:** Investigation. **Marjorie Fournier:** Formal analysis; investigation. **Andre Furger:** Supervision; funding acquisition. **Shona Murphy:** Conceptualization; supervision; funding acquisition; investigation; writing – original draft; project administration; writing – review and editing.

In addition to the [CRediT](#) author contributions listed above, the contributions in detail are:

MT performed all the experiments and bioinformatics analysis except for the following: initial help with the mNET-seq from JZ and TN, JN performed the 3' READS libraries preparation and sequencing, SH processed the phosphoproteomics samples, and MF processed and analyzed the SF3B1 proteomics samples. AF supervised JN. SM made the CDK9as cell line, carried out the cell proliferation analyses and supervised MT and JZ. MT and SM wrote the manuscript.

Disclosure and competing interests statement

The authors declare that they have no conflict of interest.

References

- Bandiera R, Wagner RE, Britto-Borges T, Dieterich C, Dietmann S, Bornelov S, Frye M (2021) RN7SK small nuclear RNA controls bidirectional transcription of highly expressed gene pairs in skin. *Nat Commun* 12: 5864
- Bensaude O (2011) Inhibiting eukaryotic transcription: Which compound to choose? How to evaluate its activity? *Transcription* 2: 103–108
- Bernecky C, Pitzko JM, Cramer P (2017) Structure of a transcribing RNA polymerase II-DSIF complex reveals a multidentate DNA-RNA clamp. *Nat Struct Mol Biol* 24: 809–815
- Bishop AC, Ubersax JA, Petsch DT, Matheos DP, Gray NS, Blethrow J, Shimizu E, Tsien JZ, Schultz PG, Rose MD et al (2000) A chemical switch for inhibitor-sensitive alleles of any protein kinase. *Nature* 407: 395–401
- Buratowski S (2009) Progression through the RNA polymerase II CTD cycle. *Mol Cell* 36: 541–546
- Castelo-Branco G, Amaral PP, Engstrom PG, Robson SC, Marques SC, Bertone P, Kouzarides T (2013) The non-coding snRNA 7SK controls transcriptional termination, poisoning, and bidirectionality in embryonic stem cells. *Genome Biol* 14: R98
- Cooke C, Hans H, Alwine JC (1999) Utilization of splicing elements and polyadenylation signal elements in the coupling of polyadenylation and last-intron removal. *Mol Cell Biol* 19: 4971–4979
- Corden JL (2013) RNA polymerase II C-terminal domain: Tethering transcription to transcript and template. *Chem Rev* 113: 8423–8455
- Cortazar MA, Sheridan RM, Erickson B, Fong N, Glover-Cutter K, Brannan K, Bentley DL (2019) Control of RNA Pol II speed by PNUTS-PP1 and Spt5 dephosphorylation facilitates termination by a "Sitting Duck Torpedo" mechanism. *Mol Cell* 76: 896–908.e4
- Crooks GE, Hon G, Chandonia JM, Brenner SE (2004) WebLogo: a sequence logo generator. *Genome Res* 14: 1188–1190
- Czudnochowski N, Bosken CA, Geyer M (2012) Serine-7 but not serine-5 phosphorylation primes RNA polymerase II CTD for P-TEFb recognition. *Nat Commun* 3: 842
- Davidson L, Muniz L, West S (2014) 3' end formation of pre-mRNA and phosphorylation of Ser2 on the RNA polymerase II CTD are reciprocally coupled in human cells. *Genes Dev* 28: 342–356
- Decker TM, Forne I, Straub T, Elsaman H, Ma G, Shah N, Imhof A, Eick D (2019) Analog-sensitive cell line identifies cellular substrates of CDK9. *Oncotarget* 10: 6934–6943
- Dobin A, Davis CA, Schlesinger F, Drenkow J, Zaleski C, Jha S, Batut P, Chaisson M, Gingeras TR (2013) STAR: ultrafast universal RNA-seq aligner. *Bioinformatics* 29: 15–21
- Dye MJ, Proudfoot NJ (1999) Terminal exon definition occurs cotranscriptionally and promotes termination of RNA polymerase II. *Mol Cell* 3: 371–378
- Eaton JD, Francis L, Davidson L, West S (2020) A unified allosteric/torpedo mechanism for transcriptional termination on human protein-coding genes. *Genes Dev* 34: 132–145
- Eifler TT, Shao W, Bartholomeeusen K, Fujinaga K, Jager S, Johnson JR, Luo Z, Krogan NJ, Peterlin BM (2015) Cyclin-dependent kinase 12 increases 3' end processing of growth factor-induced c-FOS transcripts. *Mol Cell Biol* 35: 468–478
- Fianu I, Chen Y, Dienemann C, Dybkov O, Linden A, Urlaub H, Cramer P (2021) Structural basis of Integrator-mediated transcription regulation. *Science* 374: 883–887
- Ghamari A, van de Corput MP, Thongjuea S, van Cappellen WA, van Ijcken W, van Haren J, Soler E, Eick D, Lenhard B, Grosveld FG (2013) *In vivo* live imaging of RNA polymerase II transcription factories in primary cells. *Genes Dev* 27: 767–777
- Greifenberg AK, Honig D, Pilarova K, Duster R, Bartholomeeusen K, Bosken CA, Anand K, Blazek D, Geyer M (2016) Structural and functional analysis of the Cdk13/Cyclin K complex. *Cell Rep* 14: 320–331
- Gunderson SI, Beyer K, Martin G, Keller W, Boelens WC, Mattaj LW (1994) The human U1A snRNP protein regulates polyadenylation via a direct interaction with poly(A) polymerase. *Cell* 76: 531–541
- Hoque M, Ji Z, Zheng D, Luo W, Li W, You B, Park JY, Yehia G, Tian B (2013) Analysis of alternative cleavage and polyadenylation by 3' region extraction and deep sequencing. *Nat Methods* 10: 133–139
- Hou L, Wang Y, Liu Y, Zhang N, Shamovsky I, Nudler E, Tian B, Dynlacht BD (2019) Paf1C regulates RNA polymerase II progression by modulating elongation rate. *Proc Natl Acad Sci U S A* 116: 14583–14592
- Hsin JP, Manley JL (2012) The RNA polymerase II CTD coordinates transcription and RNA processing. *Genes Dev* 26: 2119–2137
- Hu S, Peng L, Xu C, Wang Z, Song A, Chen FX (2021) SPT5 stabilizes RNA polymerase II, orchestrates transcription cycles, and maintains the enhancer landscape. *Mol Cell* 81: 4425–4439
- Huang KL, Jee D, Stein CB, Elrod ND, Henriques T, Mascibroda LG, Baillat D, Russell WK, Adelman K, Wagner EJ (2020) Integrator recruits protein phosphatase 2A to prevent pause release and facilitate transcription termination. *Mol Cell* 80: 345–358
- Jonkers I, Kwak H, Lis JT (2014) Genome-wide dynamics of Pol II elongation and its interplay with promoter proximal pausing, chromatin, and exons. *Elife* 3: e02407
- Ke S, Alemu EA, Mertens C, Gantman EC, Fak JJ, Mele A, Haripal B, Zucker-Scharff I, Moore MJ, Park CY et al (2015) A majority of m6A residues are in the last exons, allowing the potential for 3' UTR regulation. *Genes Dev* 29: 2037–2053
- Kim M, Krogan NJ, Vasiljeva L, Rando OJ, Nede A, Greenblatt JF, Buratowski S (2004) The yeast Rat1 exonuclease promotes transcription termination by RNA polymerase II. *Nature* 432: 517–522
- Kyburz A, Friedlein A, Langen H, Keller W (2006) Direct interactions between subunits of CPSF and the U2 snRNP contribute to the coupling of pre-mRNA 3' end processing and splicing. *Mol Cell* 23: 195–205

- Laitem C, Zaborowska J, Isa NF, Kufs J, Dienstbier M, Murphy S (2015) CDK9 inhibitors define elongation checkpoints at both ends of RNA polymerase II-transcribed genes. *Nat Struct Mol Biol* 22: 396–403
- Langmead B, Salzberg SL (2012) Fast gapped-read alignment with Bowtie 2. *Nat Methods* 9: 357–359
- Li H, Handsaker B, Wysoker A, Fennell T, Ruan J, Homer N, Marth G, Abecasis G, Durbin R, Genome Project Data Processing Subgroup (2009) The sequence alignment/map format and SAMtools. *Bioinformatics* 25: 2078–2079
- Martin M (2011) Cutadapt removes adapter sequences from high-throughput sequencing reads. *EMBnet J* 17: 10–12
- Medlin JE, Uguen P, Taylor A, Bentley DL, Murphy S (2003) The C-terminal domain of pol II and a DRB-sensitive kinase are required for 3' processing of U2 snRNA. *EMBO J* 22: 925–934
- Mermoud JE, Cohen P, Lamond AI (1992) Ser/Thr-specific protein phosphatases are required for both catalytic steps of pre-mRNA splicing. *Nucleic Acids Res* 20: 5263–5269
- Neve J, Burger K, Li W, Hoque M, Patel R, Tian B, Gullerova M, Furger A (2016) Subcellular RNA profiling links splicing and nuclear DICER1 to alternative cleavage and polyadenylation. *Genome Res* 26: 24–35
- Niwa M, Rose SD, Berget SM (1990) *In vitro* polyadenylation is stimulated by the presence of an upstream intron. *Genes Dev* 4: 1552–1559
- Nojima T, Gomes T, Grosso ARF, Kimura H, Dye MJ, Dhir S, Carmo-Fonseca M, Proudfoot NJ (2015) Mammalian NET-Seq reveals genome-wide nascent transcription coupled to RNA processing. *Cell* 161: 526–540
- Nojima T, Tellier M, Foxwell J, Ribeiro de Almeida C, Tan-Wong SM, Dhir S, Dujardin G, Dhir A, Murphy S, Proudfoot NJ (2018) Deregulated expression of mammalian lncRNA through loss of SPT6 induces R-Loop formation, replication stress, and cellular senescence. *Mol Cell* 72: 970–984.e7
- Pak V, Eifler TT, Jager S, Krogan NJ, Fujinaga K, Peterlin BM (2015) CDK11 in TREX/THOC regulates HIV mRNA 3' end processing. *Cell Host Microbe* 18: 560–570
- Parua PK, Booth GT, Sanso M, Benjamin B, Tanny JC, Lis JT, Fisher RP (2018) A Cdk9-PP1 switch regulates the elongation-termination transition of RNA polymerase II. *Nature* 558: 460–464
- Parua PK, Kalan S, Benjamin B, Sanso M, Fisher RP (2020) Distinct Cdk9-phosphatase switches act at the beginning and end of elongation by RNA polymerase II. *Nat Commun* 11: 4338
- Patro R, Duggal G, Love MI, Irizarry RA, Kingsford C (2017) Salmon provides fast and bias-aware quantification of transcript expression. *Nat Methods* 14: 417–419
- Perez-Riverol Y, Csordas A, Bai J, Bernal-Llinares M, Hewapathirana S, Kundu DJ, Inuganti A, Griss J, Mayer G, Eisenacher M et al (2019) The PRIDE database and related tools and resources in 2019: improving support for quantification data. *Nucleic Acids Res* 47: D442–D450
- Peterlin BM, Price DH (2006) Controlling the elongation phase of transcription with P-TEFb. *Mol Cell* 23: 297–305
- Poss ZC, Ebmeier CC, Odell AT, Tangpeerachaikul A, Lee T, Pelish HE, Shair MD, Dowell RD, Old WM, Taatjes DJ (2016) Identification of mediator kinase substrates in human cells using cortistatin A and quantitative phosphoproteomics. *Cell Rep* 15: 436–450
- Proudfoot NJ (2016) Transcriptional termination in mammals: Stopping the RNA polymerase II juggernaut. *Science* 352: aad9926
- Quinlan AR, Hall IM (2010) BEDTools: a flexible suite of utilities for comparing genomic features. *Bioinformatics* 26: 841–842
- Ramirez F, Ryan DP, Gruning B, Bhardwaj V, Kilpert F, Richter AS, Heyne S, Dundar F, Manke T (2016) deepTools2: a next generation web server for deep-sequencing data analysis. *Nucleic Acids Res* 44: W160–W165
- Rozenblatt-Rosen O, Nagaike T, Francis JM, Kaneko S, Glatt KA, Hughes CM, LaFramboise T, Manley JL, Meyerson M (2009) The tumor suppressor Cdc73 functionally associates with CPSF and CstF 3' mRNA processing factors. *Proc Natl Acad Sci U S A* 106: 755–760
- Sanso M, Levin RS, Lipp JJ, Wang VY, Greifengberg AK, Quezada EM, Ali A, Ghosh A, Larochelle S, Rana TM et al (2016) P-TEFb regulation of transcription termination factor Xrn2 revealed by a chemical genetic screen for Cdk9 substrates. *Genes Dev* 30: 117–131
- Shi Y, Reddy B, Manley JL (2006) PP1/PP2A phosphatases are required for the second step of Pre-mRNA splicing and target specific snRNP proteins. *Mol Cell* 23: 819–829
- Stuart SA, Houel S, Lee T, Wang N, Old WM, Ahn NG (2015) A phosphoproteomic comparison of B-RAFV600E and MKK1/2 inhibitors in melanoma cells. *Mol Cell Proteomics* 14: 1599–1615
- Studniarek C, Tellier M, Martin PGP, Murphy S, Kiss T, Egloff S (2021) The 7SK/P-TEFb snRNP controls ultraviolet radiation-induced transcriptional reprogramming. *Cell Rep* 35: 108965
- Tellier M, Ferrer-Vicens I, Murphy S (2016) The point of no return: the poly (A)-associated elongation checkpoint. *RNA Biol* 13: 265–271
- Tellier M, Maudlin I, Murphy S (2020a) Transcription and splicing: a two-way street. *Wiley Interdiscip Rev RNA* 11: e1593
- Tellier M, Zaborowska J, Caizzi L, Mohammad E, Velychko T, Schwalb B, Ferrer-Vicens I, Blears D, Nojima T, Cramer P et al (2020b) CDK12 globally stimulates RNA polymerase II transcription elongation and carboxyl-terminal domain phosphorylation. *Nucleic Acids Res* 48: 7712–7727
- Vagner S, Vagner C, Mattaj JW (2000) The carboxyl terminus of vertebrate poly(A) polymerase interacts with U2AF 65 to couple 3'-end processing and splicing. *Genes Dev* 14: 403–413
- Vervoort SJ, Welsh SA, Devlin JR, Barbieri E, Knight DA, Offley S, Bjelosevic S, Costacurta M, Todorovski I, Kearney CJ et al (2021) The PP2A-Integrator-CDK9 axis fine-tunes transcription and can be targeted therapeutically in cancer. *Cell* 184: 3143–3162.e32
- Vos SM, Farnung L, Boehning M, Wigge C, Linden A, Urlaub H, Cramer P (2018a) Structure of activated transcription complex Pol II-DSIF-PAF-SPT6. *Nature* 560: 607–612
- Vos SM, Farnung L, Urlaub H, Cramer P (2018b) Structure of paused transcription complex Pol II-DSIF-NELF. *Nature* 560: 601–606
- Washington K, Ammosova T, Beullens M, Jerebtsova M, Kumar A, Bollen M, Nekhai S (2002) Protein phosphatase-1 dephosphorylates the C-terminal domain of RNA polymerase-II. *J Biol Chem* 277: 40442–40448
- West S, Gromak N, Proudfoot NJ (2004) Human 5' → 3' exonuclease Xrn2 promotes transcription termination at co-transcriptional cleavage sites. *Nature* 432: 522–525
- Yamada T, Yamaguchi Y, Inukai N, Okamoto S, Mura T, Handa H (2006) P-TEFb-mediated phosphorylation of hSpt5 C-terminal repeats is critical for processive transcription elongation. *Mol Cell* 21: 227–237
- Zaborowska J, Egloff S, Murphy S (2016) The pol II CTD: new twists in the tail. *Nat Struct Mol Biol* 23: 771–777
- Zhang C, Lopez MS, Dar AC, Ladow E, Finkbeiner S, Yun CH, Eck MJ, Shokat KM (2013) Structure-guided inhibitor design expands the scope of analog-sensitive kinase technology. *ACS Chem Biol* 8: 1931–1938
- Zheng H, Qi Y, Hu S, Cao X, Xu C, Yin Z, Chen X, Li Y, Liu W, Li J et al (2020) Identification of Integrator-PP2A complex (INTAC), an RNA polymerase II phosphatase. *Science* 370: eabb5872



License: This is an open access article under the terms of the [Creative Commons Attribution](https://creativecommons.org/licenses/by/4.0/) License, which permits use, distribution and reproduction in any medium, provided the original work is properly cited.